AD-A069 211 FOSTER-MILLER ASSOCIATES INC WALTHAM MASS F/G 1/3
AN INNOVATIVE FRICTION AND WEAR TEST FOR AIRCRAFT TIRES.(U)
NOV 72 K M CAPTAIN, V K STOKES, J H EDWARDS F33657-71-C-1024
UNCLASSIFIED WP-7141 ASD-TR-72-85 NL

1 OF 2
AD A069211

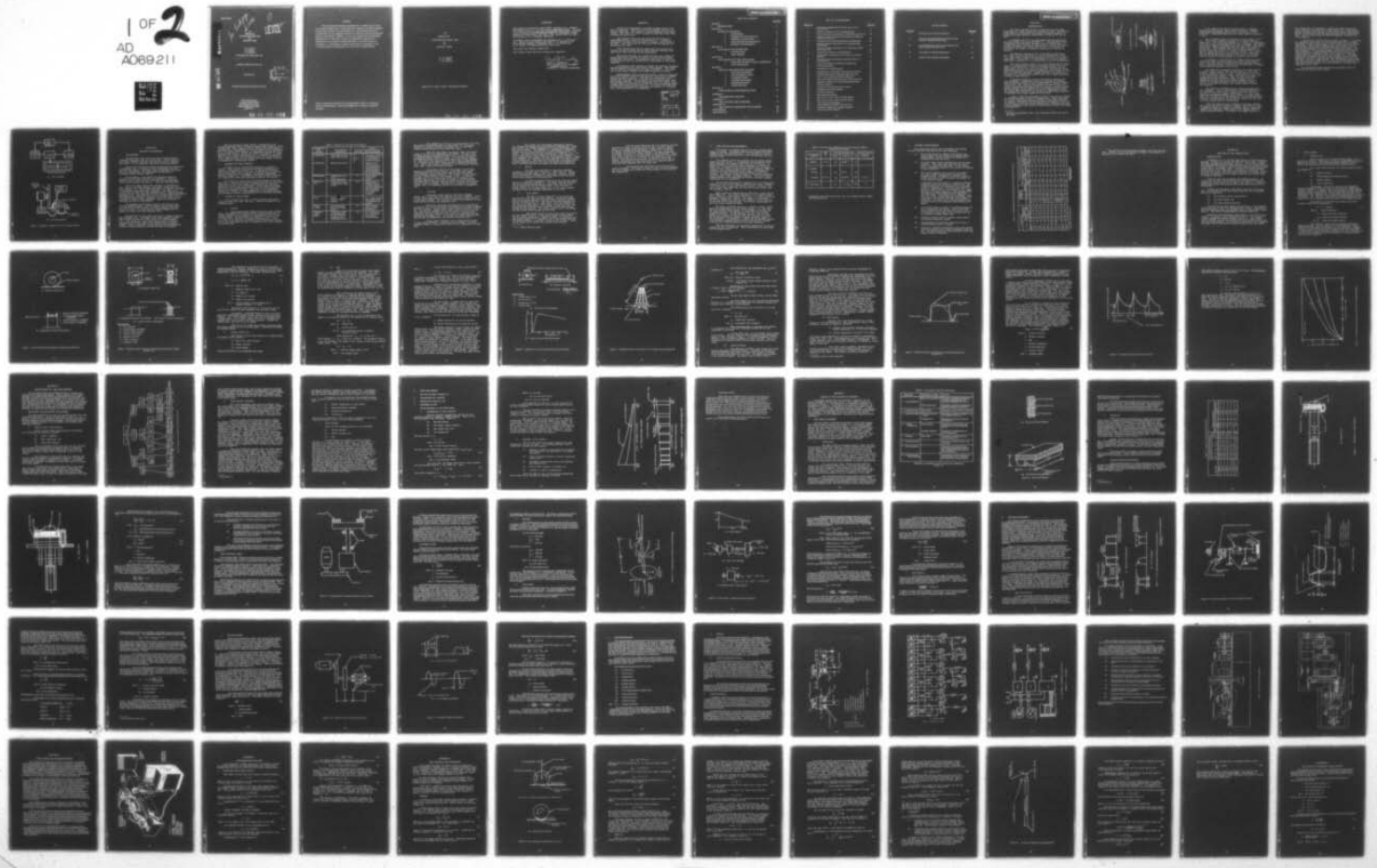

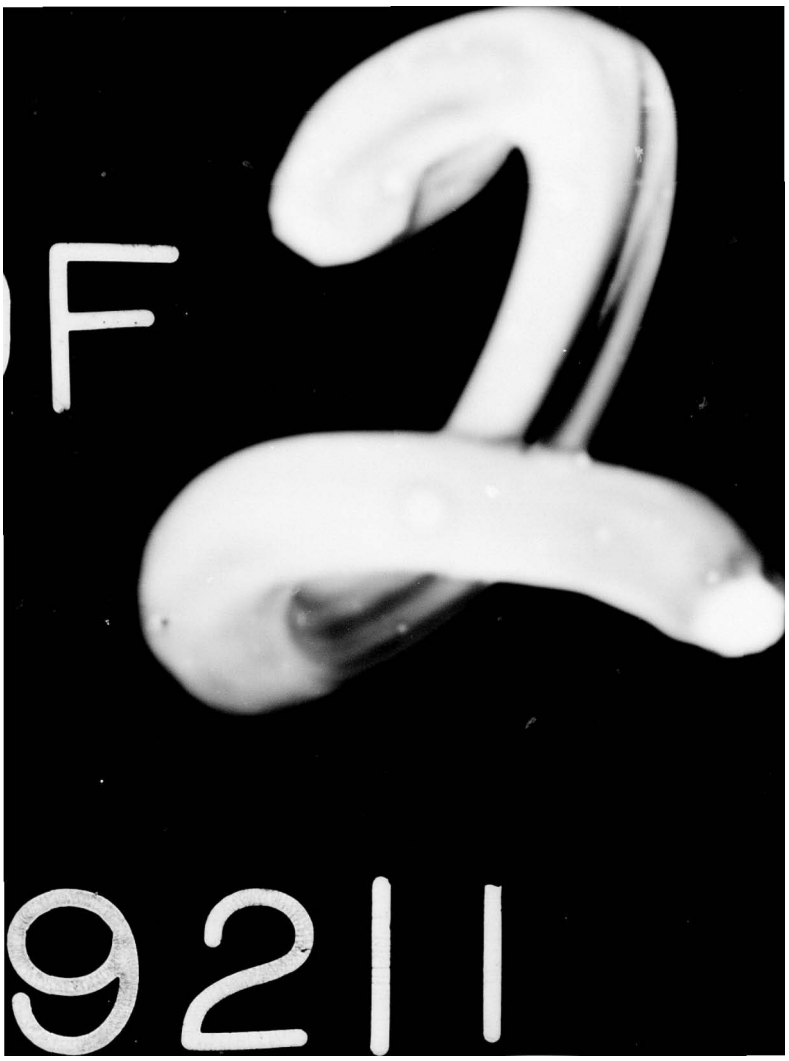
F
9211

AN INNOVATIVE FRICTION AND WEAR TEST FOR AIRCRAFT TIRES

K. M. CAPTAIN
V. K. STOKES
J. H. EDWARDS

FOSTER-MILLER ASSOCIATES, INC.

TECHNICAL REPORT ASD-TR-72-85

November 1972

Deputy for Engineering
Aeronautical Systems Division
Air Force Systems Command
Wright Patterson Air Force Base
Ohio 45433

NOTICE

When Government drawings, specifications, or other data are used for any purpose other than in connection with a definitely related Government procurement operation, the United States Government thereby incurs no responsibility nor any obligation whatsoever; and the fact that the government may have formulated, furnished, or in any way supplied the said drawings, specifications, or other data, is not to be regarded by implication or otherwise as in any manner licensing the holder or any other person or corporation, or conveying any rights or permission to manufacture, use, or sell any patented invention that may in any way be related thereto.

Copies of this report should not be returned unless return is required by security considerations, contractual obligations, or notice on a specific document.

AN
INNOVATIVE
FRICTION AND WEAR TEST
FOR
AIRCRAFT TIRES

K. M. Captain
V. K. Stokes
J. H. Edwards

FOREWORD

This report was prepared by Foster-Miller Associates, Inc., Waltham, Massachusetts on U. S. Air Force Contract F33657-71-C-1024. The work was carried out between June 1971 and November 1972 and was sponsored by the Aeronautical Systems Division, Deputy for Engineering, Wright-Patterson Air Force Base, Ohio 45433. The contract effort was under the direction of D. E. Williams, ASD/ENFL.

The authors wish to acknowledge the assistance of E. L. Foster and A. C. Harvey of Foster-Miller Associates, D. N. Wormley of the Massachusetts Institute of Technology, and D. E. Williams and H. K. Brewer of Wright-Patterson Air Force Base.

This report was submitted August 1972.

This technical report has been reviewed and is approved.

David B Tremblay

DAVID B. TREMBLAY
Chief, Landing Gear & Mechanical
Equipment Division
Directorate of Airframe Engineering

ABSTRACT

Aircraft tire performance is presently evaluated mainly on the basis of tread wear. Most low-wear tread compounds also have low friction coefficients. This results in a longer stopping distance during landing. Thus, there is a need to evaluate aircraft tires on the basis of friction as well as wear.

This program is the first step toward the formulation of a standardized test for aircraft tire friction and wear. A method is determined to evaluate tire performance by testing a small section of the tread. This reduces the size and cost of the test equipment and shortens the test time.

Tread loading during takeoff, landing and cornering has been analyzed in order to identify the operating conditions resulting in the most severe tread wear and friction requirements.

The factors that affect tire friction and wear were studied and the dominant forces, motions and heating of a tread element during landing were determined. The analysis was then used as a basis for the formulation of the test method and the requirements for the testing equipment.

A machine has been designed to simulate the significant mechanical and thermal loading on the tread element during landing. This machine will be capable of evaluating the full range of current tire sizes under dry and wet runway conditions and ambient temperature extremes.

Implementation of this concept will provide a rapid and economical tire testing capability which will evaluate tires on the basis of stopping distance as well as tread life. This will be an improvement over present tests since both wear and friction will be evaluated under simulated landing conditions. It will simplify and reduce the expense of the present method of competitive tire procurement by decreasing the number of flight tests needed to evaluate the tire. It is thus recommended that this concept be implemented by fabrication and assembly of a prototype tester and demonstration of its capabilities.

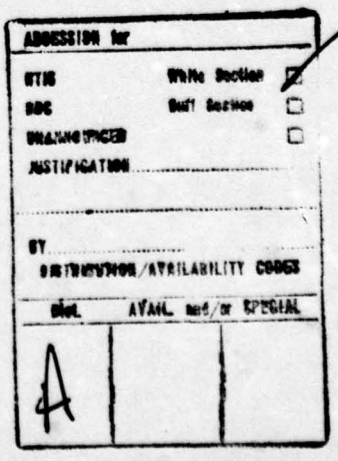

TABLE OF CONTENTS

LIST OF ILLUSTRATIONS

LIST OF TABLES

SECTION I

INTRODUCTION

This report describes the work carried out by Foster-Miller Associates, Inc., under Contract No. F33657-71-C-1024. The objective of this effort is to formulate a test method and design equipment to evaluate the friction and wear characteristics of the tread of aircraft tires.

At present, Air Force tire requirements are met through the life-cycle-costing procurement technique (1)[1]. This technique consists of evaluating tire performance through a cost per landing index. In essence, this index is obtained by dividing the tire cost by the number of landings obtained until removal from service. For any specific type of tire, the number of landings is determined by testing on an aircraft.

This approach evaluates the tire on the basis of tread wear, but it does not assess the tractive or friction characteristics of the tire. Many rubber compounds having low wear rates have low friction coefficients. In such cases, tire procurement on a cost per landing basis leads to selection of a tire having inferior tractive characteristics.

The current program (Phase I) is a first step towards the formulation of a standardized procedure for evaluating aircraft tires on the basis of wear and friction. Present tire testing machinery has the disadvantages of being very large and expensive. One objective of this effort is to implement an innovative approach which will reduce the size and cost of the test equipment. Another objective is to provide a research tool for studying experimentally some of the complex phenomena of rubber friction and wear.

Performance testing of tires on an aircraft is expensive and time consuming. Although such testing will inevitably be required, effective laboratory tests will reduce significantly the number of flight tests needed. The results of this program will form the basis of a specific procurement requirement which will ensure a minimum friction coefficient under various conditions of tire operation and will evaluate also the wearing characteristics of the tread. Implementation of the test method with a laboratory type machine will allow rapid comparison of alternative tires during competitive procurement.

Figure 1 shows the mechanism by which an aircraft tire supports the load and generates tractive or braking forces. These forces arise as a result of the normal and shear stresses at the contact interface or footprint. Summation of the normal stress components over the contact area gives rise to the vertical support force. Similarly, the shear stress components (in the direction of motion) add up to give the braking or tractive force.

---

[1] Numbers in parentheses refer to the references listed at the end of the report.

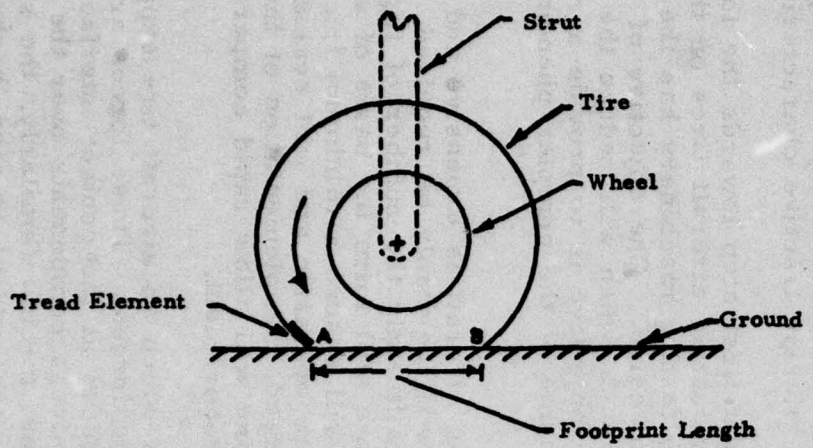

(a) Side View

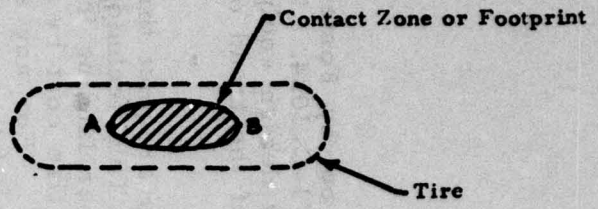

(b) Plan View in Ground Plane

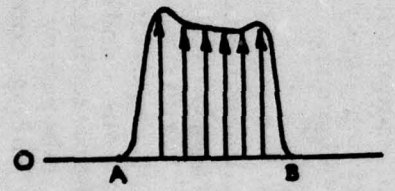

(c) Normal Stress Distribution (along footprint center)

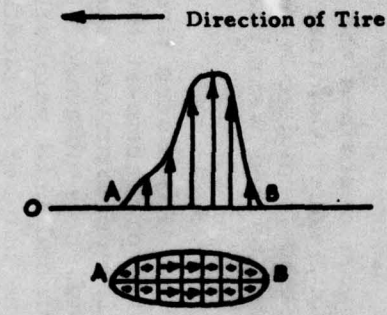

(d) Shear Stress Components (in rolling direction)

Figure 1 . Generation of Support and Tractive Forces in an Aircraft Tire

In the contact zone, there is relative motion, or slippage, between the ground and the various parts of the tread. The interaction between the slippage and the contact stresses gives rise to tread wear. Outside the contact zone, of course, there is no friction or wear.

Let us consider a small tread element on the periphery of the tire. This element, labelled A in Figure 1, is about to enter the contact zone. As it passes through this zone it experiences deformation due to the stresses, and heating and wear due to slippage. The stresses, deformations, slippage and heating vary from point to point within the contact zone. After emerging from this zone (point B in Figure 1), the element is free of surface shear until it reaches position A as before. During this period, i.e., when the element is not in contact with the ground, there are no friction forces or wear. The main effect on the element during this part of the cycle is heat transfer from the element to the surroundings and conduction into the tire.

In summary, a tread element of a loaded rotating tire passes through two zones; the ground contact zone and the out-of-contact zone. The contact zone is characterized by high tangential (friction) stresses and heat generation, while the out-of-contact zone is characterized by significant amounts of heat transfer.

One approach to developing a laboratory test method would be to isolate a small portion of the tread and subject it to the same stresses, slippage, heating, etc. that it would experience as part of a tire during landing, takeoff, taxiing, cornering and so forth. Such an approach has two drawbacks. First, the stress distributions, slippage and thermal interactions within the footprint are not sufficiently well known for all the loading conditions of the tire. Second, even if these phenomena could be described in detail, a machine to simulate them under every loading condition would be very expensive.

Our approach to developing the test method is simpler and more pragmatic. There is much evidence (2) to show that most tires are removed from service due to (uniform) excessive tread wear. This type of wear occurs mainly during landing. It is also during landing that the highest available friction forces are usually required. Thus, as a starting point in the development, the test machine can be designed to simulate landing and measure the friction force and wear of a tread element while it is being braked.

There are numerous force, deflection and thermal conditions that must be duplicated to simulate a landing. Here again, an order-of-magnitude analysis can identify the dominant effects. When these conditions are simulated, useful results can be obtained without an unduly complicated design. For instance, the slipping velocity of a

tread element has two components: primary slip along the direction of tire motion and secondary slip at right angles to it. During normal landing, secondary slip is known to be very much smaller than primary slip (3), so that most of the wear during braking will be caused by the latter. Thus, at least during the initial development, secondary slip can be neglected.

A sketch of the machine concept is shown in Figure 2. It consists of a rotating pavement table, the tread element under test, a loading mechanism, an input control system, and the friction and wear measurement system. The pavement simulates the runway surface, and its rotation establishes the gross slippage between tire and runway. The test specimen consists of a small section of tread taken from the tire under evaluation. The loading mechanism cyclically forces the tread element against the rotating pavement and sets up the stresses and deformations that correspond to those of the loaded tire. The input control system programs the action of the pavement table and loading mechanism to simulate a specific operating condition for the tire (e.g., high speed, low gross weight landing). The measurement system measures and records the friction force, normal force and lateral force, the roll, pitch and yaw moments, the tread compression, the bulk tread temperature and the slip.

The sections that follow describe the formulation of the test method and the design of the hardware.

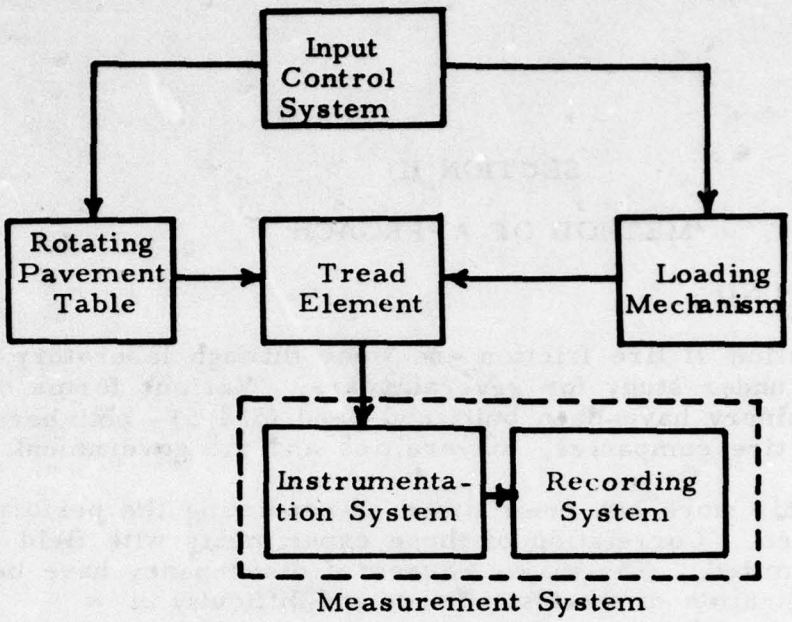

(a) Block Diagram

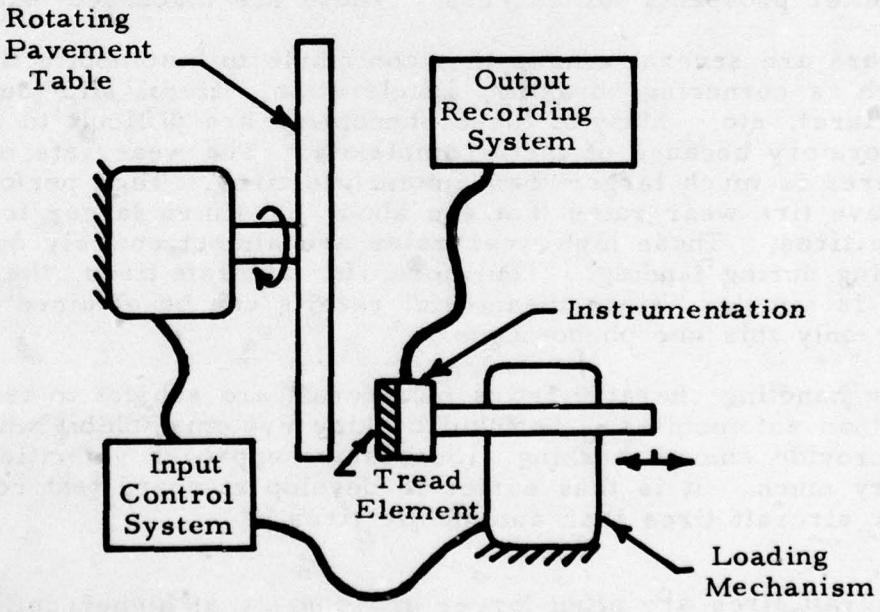

(b) Conceptual Sketch

Figure 2 Schematic Diagram of Tire Testing Machine

SECTION II

METHOD OF APPROACH

1. BACKGROUND

Determination of tire friction and wear through laboratory testing has been under study for several years. Various forms of tire testing machinery have been built and used (3, 4, 5) - both here and abroad - by tire companies, universities and the government.

Most of this work has been aimed at predicting the performance of automobile tires. Correlation of these experiments with field tests has been limited. The major causes of discrepancy have been felt to be contamination of the test surface and difficulty in simulating realistic driving conditions.

At first glance, it may appear that laboratory testing of aircraft tires will suffer from the same drawbacks. There are however several factors peculiar to aircraft tire operation which indicate better prospects for success. These are discussed below.

There are several effects that contribute to automobile tire wear, such as cornering, braking, acceleration, lateral slip (due to tire curvature), etc. Many of these phenomena are difficult to simulate in the laboratory because of their complexity. The wear rate of aircraft tires is much larger than automobile tires. High performance aircraft have tire wear rates that are about 100 times larger than those of automobile tires. These high wear rates are almost entirely due to hard braking during landing. Therefore, for aircraft tires, the test procedure is simpler, since meaningful results can be obtained by simulating only this one phenomenon.

The handling characteristics of aircraft are subject to less variation than automobiles. Antiskid braking systems inhibit wheel lock and provide smooth braking. Successive approach velocities do not vary much. It is thus easier to develop standard test conditions for aircraft tires than automobile tires.

Aircraft tires are often larger and operate at higher deflections than automobile tires. The bigger contact areas suggest that edge effects within the footprint are less severe than with automobile tires. Thus testing of a small tread element based on conditions prevailing in the central region of the footprint will have greater validity. There is, therefore, reason to believe that implementation of the new testing concept for aircraft tires will be successful.

With any laboratory testing machine, contamination of the simulated pavement surface, caused by abraded rubber particles, should be minimized. When compared with the rotating drum dynamometer, pavement surface contamination for the new machine will be significantly less. The extent of the reduction in contamination will depend on the pavement table diameter, and the size of the tread element. A simple analysis of the average contamination level is presented in Appendix I. Over a range of typical tire and machine sizes, the average thickness, of the contaminant layer will be reduced by a factor between 4 and 20, as compared to a rotating drum machine.

2. REASONS FOR TIRE REMOVAL

Aircraft tires are removed from service for a variety of reasons. These reasons and a typical percentage breakdown of the returns are summarized in Table I (2). In any specific situation, more precise figures for tire removal will depend on local conditions, such as runway layout and roughness, aircraft type and handling technique, weather, etc. Nevertheless, the data of Table I can serve as a rough guide to determine the primary causes of tire removal.

As can be seen, most tires are removed because of excessive tread wear. About 80 percent of all tires are removed for this reason. Other reasons, such as cut treads or braking flats are much less significant. This is easy to understand. Tread cutting and braking flats occur due to sharp stones on the runway and brake malfunction. They can be minimized by better runway and aircraft maintenance. Braking wear, however, is more fundamental to the landing process, and can only be reduced by improvements in tire materials and design.

3. CAUSES OF TREAD WEAR

For an aircraft tire, there are four conditions under which abrasion of the tread rubber can occur. These are discussed in the following section.

a. Braking

Hard braking during landing is the main cause of tread wear. The braking force arises at the tire-runway interface and is strongly dependent on the coefficient of friction between the two contacting surfaces. During braking, the peripheral velocity of a tire is a little slower than that of a similar free-running tire. This occurs due to tire elasticity and relative motion at the contact interface. This (percentage) decrease in peripheral velocity due to braking is called the slip.

Table I Reasons for Aircraft Tire Removal

Reasons for Tire Removal	Description of Tread Surface	Percent Removed	Typical Operational and/or Runway Conditions
Tread Wear	Fine ridges or saw-tooth cross-section	80.3	Cornering, tractive or braking forces on dry textured abrasive runways
Tread Wear	Smooth to the touch		Medium to low frictional forces and movements in many directions. Arises mainly on smooth textured dry or wet runways
Braking flat	A flattening of the tread circumferentially	2.1	Locked wheel skid on dry runway
Scored or cut	Long or short cuts in otherwise smooth surface	15.9	High tractive or braking effect on runways containing sharp aggregate and loose flints. Also touchdown on similar surfaces
Torn	Chunks of rubber torn out of the surface	--	Dry, rough runways when high driving or braking forces applied
Groove cracks	Cracks along the base of the tread groove	0.9	High stressing during airport manoeuvers
Reverted rubber patch	A thin skin, which can be peeled off the tread leaving a rough porous substratum visible	0.8	Non-rotating tire on a low friction wet surface, usually flooded

The coefficient of friction is a strong function of the slip and reaches its maximum value at a slip between 15 ~ 20 percent. Therefore, in order to minimize the landing roll, aircraft brake systems usually maintain the slip within this range.

When the wheel brakes are applied, most of the kinetic energy of the aircraft is dissipated in the brakes. The bulk of the remaining energy is dissipated through the tire, and a small amount is dissipated through aerodynamic drag. The proportion of energy dissipated through the tires is roughly equal to the slip (see Appendix II). Therefore, after application of the wheel brakes, approximately 15 ~ 20 percent of the initial kinetic energy is dissipated through the tires. Most of this energy is dissipated at the tread-runway interface, which leads to high local heating and wear.

The present trend in aircraft design is toward higher approach speeds and heavier aircraft. At the same time, space restrictions have led to multi-wheel undercarriages with smaller tires and higher inflation pressures. The net effect of these factors has been a sharp increase in tire loading. Today, aircraft tire pressures are 5 to 10 times larger than those of automobile tires. Although improvements in aircraft tire design and tread compounds have taken place, these have not been able to counteract the increased severity of the tire loading. This has led to increased wear during landing, with a corresponding decrease in the number of landings per tire.

b. Cornering

Cornering can also result in tread wear, although usually, this is much less severe than the wear due to braking. Cornering wear occurs when there is a side force on the tire which causes it to yaw and/or sideslip. The side force causes tread movement, or slip, in the lateral direction, thus resulting in wear.

Tests have shown that cornering wear is proportional to the $(\text{side force})^n$, where the exponent (n) depends on the runway roughness and the tire design. Typical values of this exponent lie between 2 and 3 (2). The side force depends on the radius of the turn and the velocity. Thus both of these variables will have an effect on cornering wear, particularly the latter, because of the square law relationship between velocity and centrifugal force. Part of the wear during crosswind landings will also be generated by the mechanism described above.

Under unusual conditions, such as high speed turn-offs or tight ground maneuvers, cornering wear can be high. In normal operation, however, cornering wear will not be as significant as braking wear.

The results of an approximate mathematical analysis for cornering and braking wear are presented in Reference (2). Using these results, the relative magnitudes of cornering and braking wear have been estimated. This comparison is summarized in Appendix II. Braking wear has been evaluated for a normal landing under dry conditions. Cornering wear has been estimated for a single 90° turn. The radius of the turn has been assumed as one-tenth of the landing roll, with a turning velocity equal to one-tenth of the approach velocity. Under these conditions, the cornering wear was estimated to be about 6 percent of the braking wear. This figure will increase due to successive turns and other parking maneuvers, but since the velocity will probably be lower, cornering wear will still remain well below the braking wear.

c. Spin Up

Tire spin up at touchdown has often been identified mistakenly as a major cause of tire wear. This is not so. During spin up, the peak wear rate is likely to be high. However, because of the short duration, the volume of rubber abraded from the tread will be small compared to the braking wear.

An order-of-magnitude analysis for the work done during spin up is presented in Appendix II. The results show that the work done by tire friction during spin up is only about 2 percent of the energy dissipated by the tire during braking. Since tire wear is closely linked to the frictional energy loss, one can safely conclude that spin up does not contribute significantly to tire wear.

d. Free Rolling

The wear of a free rolling tire[2] is very much less than that due to any other operating condition. During free rolling, most of the energy required to overcome rolling resistance goes into hysteretic heating of the tire. This changes the bulk temperature of the tire, but in itself does not cause wear. Some slip between tire and runway also takes place. This slippage is relatively small, and occurs when the (curved) surface of the tire deforms while passing through the (flat) footprint. The relative motion results in an energy loss and causes surface heating and tread wear.

The energy loss due to slip is only about 10 percent of the total rolling losses (3). These losses depend on many factors such as velocity, temperature, inflation pressure, tire deflection, etc. Experimental studies (3) of automobile tires at high speeds show that the rolling resistance is less than 5 percent of the tire load. Experimental results (7) for aircraft tires confirm this conclusion.

---

[2] i.e., without external torque.

From the above discussion, the force needed to overcome slip losses is about 1/2 percent of the tire load. In more familiar terms, a tire rolling freely operates at a slip of about 1/2 percent. In contrast, braking slip during landing is between 15 ~ 20 percent. The energy lost at the tire-runway interface, is roughly proportional to the slip. Tread wear is closely related to this energy loss. Therefore, when an aircraft tire is rolling free, the energy lost in the footprint is only about 1/30 to 1/40 of the corresponding loss during braking. Even though taxiing distances can be two to three times as much as the braking roll, tread wear while free rolling will still be very small when compared with the braking wear.

During takeoff, the only torque on the tire is due to wheel acceleration. This torque is small, so that, practically speaking, the tire is rolling free, so that wear during takeoff is very much less than landing wear.

4. TIRE FRICTION REQUIREMENTS

Tire friction is important when the aircraft is braking (wheel brakes) or turning. The highest friction forces required are during landing to limit the stopping distance. The maximum tire friction available during braking is thus one of the most important characteristics of a tire.

The maximum friction force between the tire and the runway depends on many factors. It is influenced by the properties of the tread compound, the condition of the tread, the tire velocity, the inflation pressure, the runway surface properties, the presence of water, etc. A reduction in the friction coefficient due to changes in any of these factors can have serious effects, especially under wet conditions, when stopping distances are large. Measurement of friction forces under simulated landing conditions is, therefore, essential. An estimate can then be made of the stopping capabilities of the tire under various operating conditions. This can be used to evaluate different tread compounds and develop a minimum stopping requirement for tire qualification.

The preceding discussion has explained why tire braking during landing is the most severe loading condition for the tread. Braking is the main cause of tread wear and tire removal. Normally, this wear is many times higher than the wear due to other causes, such as cornering or spin up.

These results are summarized in Table II for a typical takeoff and landing cycle. The relative magnitudes of the frictional energy loss -- which is a rough measure of tire wear -- is shown for takeoff, touchdown, braking and cornering. The figures are approximate, but they do confirm that, under normal conditions, a very large part of tire wear occurs during landing. Tire friction requirements are also most severe during this period.

The above conclusions permit us to establish realistic requirements for development of the new testing concept. As a first step, the tread element testing machine can be designed to simulate only the braking portion of the landing roll rather than every loading condition of the tire. By this approach, the size, cost and complexity of the machine is reduced, while still being able to provide the friction and wear data needed to evaluate the major aspects of tire performance. As experience is gained with the operation and use of the machine, additional features can be incorporated to simulate cornering and crosswind landing and study other phenomena.

With this background, the operational requirements for the new machine can now be established. These requirements are enumerated in the following section.

Table II Tire Friction Coefficients and Losses During Takeoff, Landing and Cornering

Tire Operating Condition	Slip (s) %	Frictional Energy Loss			Typical friction coefficients required
		Symbol	Equation	%*	
1. Takeoff	~ 1/2	E_T	$\frac{1}{2} MV^2 s$	3%	-
2. Landing					
Spin up	-	E_s	$\frac{1}{2} I \omega^2$	2%	-
Braking	15 ~ 20	E_B	$\frac{1}{2} MV^2 s$	80%	0.2~0.6
3. Cornering	-	E_c	$.1 \sim .2 E_B$	15%	0.1

*Computed on the total friction loss over one complete takeoff, landing and cornering cycle.

5. MACHINE REQUIREMENTS

After discussions with Air Force personnel, the following principal operating requirements have been established.

(1) The machine should be capable of forcing the tread element against the test pavement to simulate braking during landing. Details of the forcing function are developed in Sections III and IV.

(2) The tread element will be obtained from the tire under evaluation. This requirement eliminates the need to prepare any special test specimens. It also ensures that the compounding formula of the test piece is identical to that of the tire.

(3) The machine should be able to test the full range of tire sizes at their normal inflation pressures and touchdown speeds. In addition, it should be capable of testing most tires at higher pressures and speeds, up to the maximum rating.

A tabulation of the parameters of a number of different military aircraft tires is shown in Table III (8). The method by which the tread parameters were calculated is given in Appendix III. As can be seen, there are a few tires, such as the 56 x 16 and the 20 x 4.4, which operate at very large pressures or high rotating speeds. The highest machine loading will occur when these tires are tested. The machine will be designed to test such tires at their normal pressures and speeds. Most of the other tires operate under less severe loading conditions. For these tires, it will be possible to conduct the tests up to the maximum rated pressures and speeds.

(4) The machine should be capable of simulating braking slip up to a maximum of 20 percent. Since all anti-skid brake systems keep the slip below 20 percent, there is no justification at this time for the increased size and cost needed to simulate higher slips.

(5) Provision should be made to simulate runway wetness and ambient temperature change.

(6) Interchangeable test pavements should be provided, to simulate different types of runways.

(7) The forces, moments and deflection of the tread element should be measured and recorded continuously during the test. The bulk temperature and slip velocity of the tread element should be monitored.

Table III Tire Specifications and Tread Parameters for Some Common Aircraft Tires

Tire Specifications				Aircraft	Footprint Dimensions		Contact Ratio* %	Tread Element Contact Parameters			
								For a Landing speed of 150 mph		For Maximum rated Tire Speed	
Tire Size	Ply Rating	Loaded Inflation Pressure (lb/in^2)	Max. Tire Speed (mph)		Length (in)	Area (in^2)		Minimum Contact Time (secs)	Max. Contact Frequency (hz)	Minimum Contact Time (secs)	Max. Contact Frequency (hz)
56x16	38	328	250	B-52	25	262	7.0	0.0095	15	0.0057	25
49x17	26	177	225	C-5A	23	257	6.7	0.0087	17.3	0.0058	26
44x16	28	208	200	C-141	20	209	6.8	0.0076	19.5	0.0057	26
36x11	24	244	250	F-105	16.3	121	6.8	0.0062	24	0.0037	40
32x8.8	24	348	275	F-101 A, C	13.5	81.5	7.2	0.0051	27	0.0028	50
31x11.5-16	22	286	275	F-101 B	13.8	95	7.1	0.0051	27	0.0028	50
30x11.5-14.5	24	255	247	F-4 C, J	13.7	95	6.9	0.0052	28.6	0.0032	47
30x8.8	22	307	250	F-100 F-102 F-106	13.7	83.6	7.0	0.0052	27.6	0.0031	46
25x6.75	18	312	275	F-104	10.4	44	7.6	0.0038	33.3	0.0021	61
20x4.4	12	234	225	T-38	8	23	7.9	0.003	42	0.002	63

Data adapted from Reference (8)

*$\frac{\text{Tire Circumference}}{\text{Footprint Length}}$

The machine has been designed according to the above specifications. Details of the test method and the design of the hardware are described in the sections that follow.

SECTION III

ANALYSIS OF THE BRAKED TIRE

1. INTRODUCTION

A pneumatic tire is a toroidal shell made up of several structural elements. Of these, the carcass and tread are the two basic components that affect the dynamic performance of the tire. The carcass is made up of many flexible filaments of high modulus cord, such as natural textile or glass fibre. The tread is made up of low modulus polymeric material, usually natural and synthetic rubber. Normally, the Young's Modulus of the carcass is 100 ~ 1000 times larger than that of the tread. Since the tread and carcass crossections are comparable, the inflation pressure forces (of an unloaded tire) are resisted by the carcass, and the tread is virtually stress-free.

These two main tire components have different functions. The carcass must be able to deform locally and yet transmit the vertical, tangential and lateral forces to the wheel. The tread is a covering that protects the carcass from abrasion and develops high friction forces at the pavement.

A good tread must have a high friction coefficient and low wear. There are many factors that affect friction and wear, but, in general, they can be reduced to:

(1) The pavement surface characteristics

(2) The tread loading, and

(3) The tread material properties.

The important pavement surface characteristics are the roughness and the presence, if any, of a lubricating film of water. Simulation of these characteristics with a flat pavement table is comparatively straightforward. The method of implementation is described in Section V.

Simulation of the loading and heating history of the tread is more complex. An analysis of the loading and heating of a tread element as it passes through the footprint has been carried out. The dominant stress, deflection and thermal conditions that govern landing friction and wear have been identified. These results are described in the paragraphs that follow and are then used to develop the details of the test method.

2. TIRE LOADING

a. Stationary Tire

When an inflated tire is loaded statically against a flat pavement, the tread is compressed, and forms a substantially flat contact patch at the interface. The interfacial pressure depends on several factors, the most important of these being the inflation pressure.

For a tread without grooves, the contact pressure distribution depends on:

(1) Inflation pressure

(2) Tread bending and transverse shear

(3) Sidewall stiffness

(4) Tread compression

The influence of these four factors on the longitudinal pressure distribution (along the center of the footprint) is shown qualitatively in Figure 3. In general, aircraft tires operate at high inflation pressures and have thin treads. These characteristics indicate that the inflation pressure component will be much larger than the other three components. This result has been confirmed by experiments on a smooth aircraft tire (9). Therefore, the pressure distribution along the footprint center can be assumed uniform and equal to the inflation pressure.

The presence of tread grooves increases the normal pressure, which can be expressed as

$$p' = (1 + A_g/A_t)\, p \qquad (1)$$

where p - inflation pressure

p' - contact pressure at interface

A_g - groove area within footprint

and A_t - tread area within footprint

The increased contact pressure depends on the groove width and spacing. For any specific tire, these dimensions can be obtained from the design specifications or by measurement. Although the groove width and spacing vary for different tire sizes and makes, in most cases, the contact pressure increase is about 10 ~ 20% (10, 11). A sketch of the assumed pressure distribution for a statically loaded tire is shown in Figure 4.

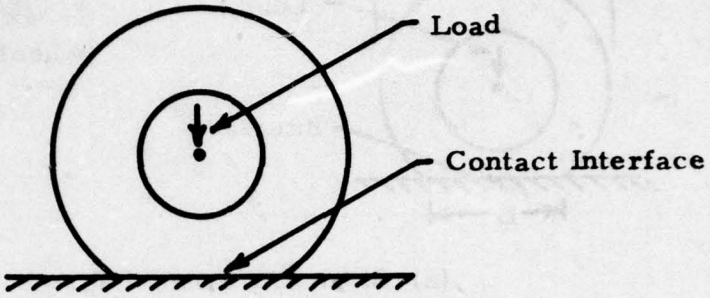

(a) Statically Loaded Tire

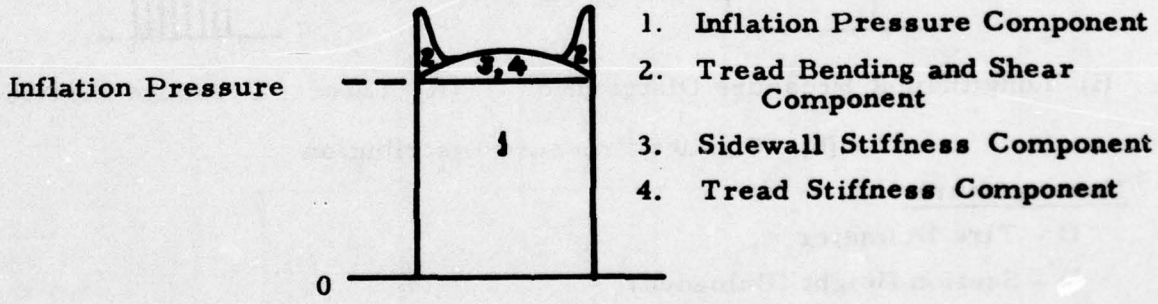

(b) Longitudinal Pressure Distribution

Figure 3 Contact Pressure Distribution for Statically Loaded Tire

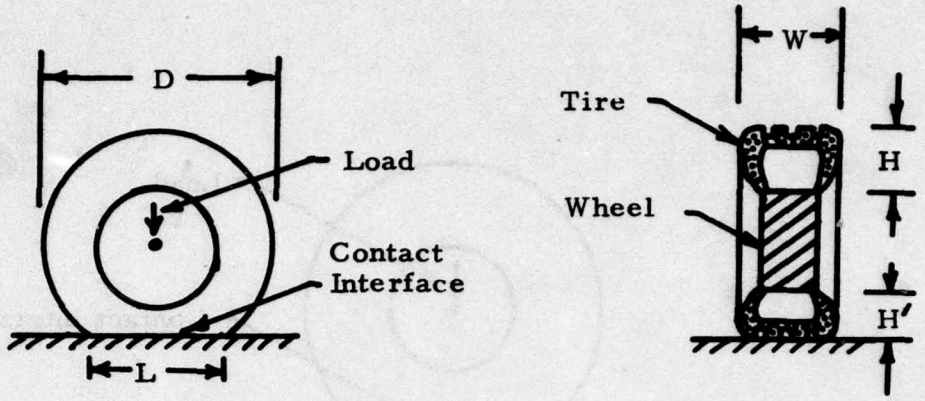

(a) Statically Loaded Tire

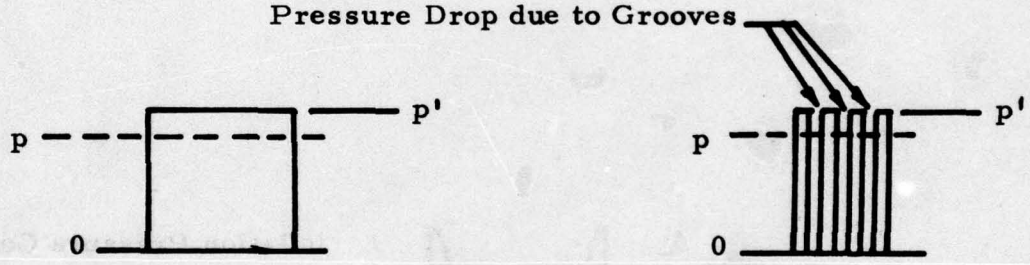

(i) Longitudinal Pressure Distribution (ii) Lateral Pressure Distribution

(b) Contact Pressure Distribution

Nomenclature

D - Tire Diameter

H - Section Height (Unloaded)

H' - Section Height (Loaded)

$\delta = 1-H'/H$ - Deflection

p - Inflation Pressure

p' - Contact Pressure

L - Footprint Length

Figure 4 Idealized Contact Pressure Distribution for Statically Loaded Aircraft Tire

The footprint of an aircraft tire has an oval shape. A classical analysis (3, 11) which considers the tire as an elastic membrane without bending stiffness, shows that the footprint area is roughly proportional to the tire deflection. The results are given below

$$A \simeq (2.3\ H\ \sqrt{D\ W})\ \delta \tag{2}$$

$$L \simeq (1.7\ \sqrt{D\ H})\ \sqrt{\delta} \tag{3}$$

where A - footprint area

L - footprint length (major axis)

D - tire diameter

H - height of tire section

W - width of tire section

and δ - percent change in section height due to loading (normally, $\delta \simeq 32\%$).

Experiments with several U. S. and German aircraft tires (3) have shown very good agreement with the above results.

In summary, a statically loaded tire has an oval footprint with a substantially uniform normal pressure across the contact interface. The stress conditions of the tread can be approximated by a simple model. In the contact region, the tread is in uniform compression with a stress equal to the contact pressure. Outside the contact region, the tread is free of stress.

When the tire is rolling and subjected to braking torque, the loading conditions of the tread will change. The effects of braking are described below.

b. Braked Rolling Tire

The friction and wear characteristics of a braked rolling tire depend on three factors:

(1) Slip at the contact interface

(2) Contact pressure

(3) Tread heating.

These are discussed in the paragraphs that follow.

(i) Slip

When a tire rolls there is always some relative velocity, or slip, between the tread and the pavement. For a tire rolling without torque, this relative motion, called secondary slip, is very small. Secondary slip occurs because of the geometrical characteristics of the toroidal tire shape. A surface of double curvature, such as a tire tread, cannot be developed. When a part of the tire enters the footprint, it can only conform to the pavement contour by local deformations of the tread and carcass. These deformations result in slip at the interface. Secondary slip is responsible for a part of the energy loss and wear during free rolling. For this type of slip, the sliding motions within the footprint are of the order of 0.01 in. (3, 4).

For a braked tire, the relative motion at the contact interface is caused by a completely different mechanism. It is a property of most rubber-like materials that the maximum friction force occurs, not at rest, but at some small slipping velocity, in the neighborhood of 1 in/sec for common tread compounds. Thus during braking, relative motion, or primary slip, occurs because the high friction forces can only be developed when there is a small but definite rubbing velocity between the tire and the pavement. Under conditions of hard braking, which is common in aircraft tires during landing, the relative motion due to primary slip is of the order of 0.1 in. This is significantly larger than the secondary slip. Thus, under braking conditions, the effects of secondary slip will be negligible.

The (absolute) slip of a tire is expressed by the change in its peripheral velocity (at the footprint) due to external torque

$$\Delta s = V_a - V_p \tag{4}$$

where Δs - absolute slip

V_a - aircraft velocity

and V_p - tire peripheral velocity at footprint (relative to axle).

When rolling free, $V_a = V_p$, so that $\Delta s = 0$. When braking, $V_a > V_p$, so that Δs is positive. The peripheral velocity at the tire footprint is the product of the rotational speed and the effective rolling radius. Thus,

$$\Delta s = V_a - r\dot{\theta} \tag{5}$$

where r - effective rolling radius of tire

and $\dot{\theta}$ - tire rotating speed.

A more useful measure of slip is the fractional slip, s.

$$s = (V_a - r\dot{\theta})/V_a \qquad (6)$$

The fractional slip indicates the relative magnitudes of rolling and slipping in a braked tire. This is shown qualitatively in Figure 5a. For instance, a free-rolling tire has zero slip, while a locked wheel condition (pure sliding) corresponds to a slip of unity.

In aircraft tires, the friction coefficient is a strong function of the slip. Usually, the friction-slip relationship has the form sketched in Figure 5b, with the maximum friction coefficient occuring at a slip (called the critical slip) in the 15 ~ 20% range. Although the maximum value of the friction coefficient depends strongly on the tire, runway and environmental conditions, the critical slip value, at which this maximum friction occurs, does not change much. Therefore, in order to obtain the maximum deceleration during landing, antiskid braking systems maintain the slip within this range.

For slips larger or smaller than the critical slip, the friction forces decrease. Roughly speaking, this is because the sliding velocity within the footprint is smaller or larger than the sliding velocity at which rubber develops its maximum friction coefficient. The above explanation is very simplified. In practice several other factors, such as tread heating, carcass deformations and water removal characteristics, enter into the picture and affect the friction-slip relationship.

For an elastic tire, the observed slip is made up of two components.

(1) Sliding between the tire and the pavement.

(2) Elastic deformation of the tread and carcass.

The sliding component of slip is simply the relative motion between the tread and the pavement, needed to develop the high friction forces. The deformation component is the change in wheel rotation caused by tangential deflections of the tread and carcass. The latter can best be explained with the help of a simplified model of the tire (4) sketched in Figure 6. In this model, the tread is idealized as a number of finite elements loaded by springs. The spring force represents the loading due to inflation pressure. As the wheel rolls, while transmitting torque, each of the elements in the footprint deforms in shear by an amount δ as shown. This causes the wheel to rotate (about its center) through an extra angle δ/R, where R is the wheel radius. Since this happens for every tread element, the extra angle of rotation, for the wheel to travel a distance equal to the tire periphery, is $n\delta/R$, where n is the total number of tread elements. The total angle of wheel rotation is thus $2\pi \pm n\delta/R$. The plus sign applies during traction and the minus sign during braking.

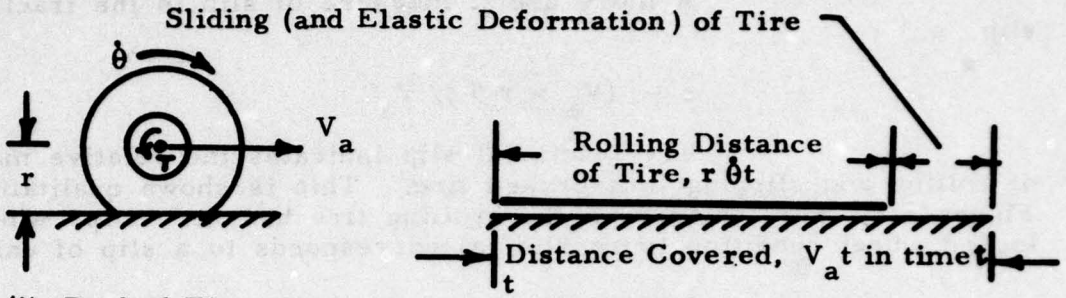

(i) Braked Tire

(ii) Distance Travelled

$$\text{Fractional Slip} = \frac{\text{Sliding Distance}}{\text{Distance Covered}} = 1 - r\dot{\theta}/V_a$$

Nomenclature

- r - rolling radius of tire
- V_a - aircraft velocity
- $\dot{\theta}$ - rotating speed of tire
- T - braking torque

(a) Description of Braking Slip

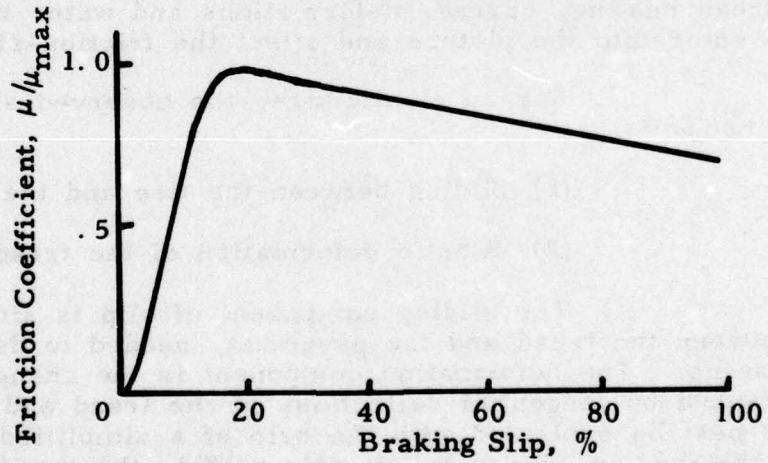

(b) Typical Friction-Slip Relationship

Figure 5 Dependence of Friction Coefficient on Braking Slip

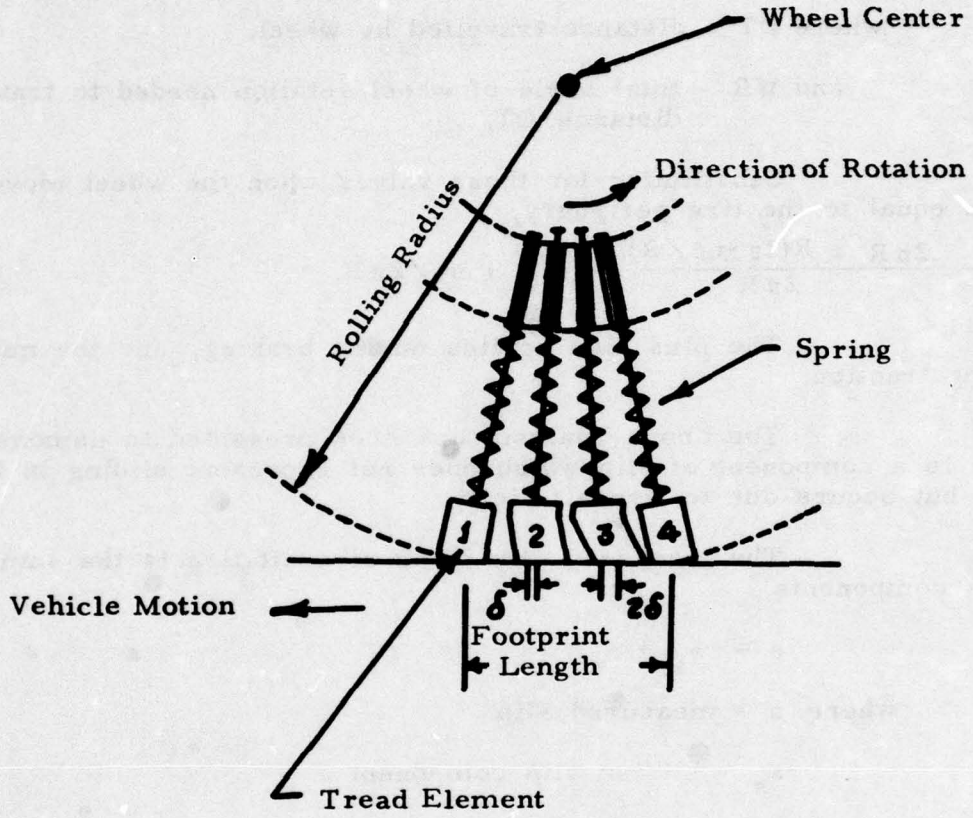

Figure 6 Simplified Model of Pneumatic Tire Running Under Braking Slip

From Equation (6), the deformation slip s_d can be rewritten as

$$s_d = \frac{DT - R \times WR}{DT} \tag{7}$$

where DT - distance travelled by wheel.

and WR - total angle of wheel rotation needed to travel distance DT.

Substituting for these values when the wheel moves a distance equal to the tire periphery,

$$s = \frac{2\pi R - R(2\pi \pm n\delta/R)}{2\pi R} = \pm n\delta/2\pi R. \tag{8}$$

The plus sign applies during braking, and the minus sign during traction.

The above analysis has been presented to demonstrate that there is a component of slip which does not represent sliding in the footprint, but occurs due to tire elasticity.

The measured slip of an aircraft tire is the sum of the two components

$$s = s_s + s_d \tag{9}$$

where s - measured slip

s_s - sliding slip component

and s_d - deformation slip component.

When simulating slip in a laboratory test machine, it is important that the general relationship between the two slip components be preserved.

For the initial tests, the tire element can be clamped at the carcass. This will allow the tread to undergo shear deformations similar to those sketched in Figure 6. If needed subsequently, carcass elasticity can be simulated by making the clamp less stiff. These considerations are discussed further in the sections relating to the clamp design.

(2) Contact Pressure

The application of braking torque changes the contact pressure distribution within the footprint. In general, an increase in speed and (braking) torque tends to increase the pressure in the front of the footprint, and reduce it at the rear. The length of the footprint is also increased slightly. The general trend of these effects is

sketched in Figure 7 and compared with the pressure distribution for a statically loaded tire.

Experiments with high speed automobile tires have shown that the increase in footprint length in the neighborhood of aircraft landing speeds is about 10%. It is expected that aircraft tires will behave similarly. However, during the high speed part of the landing, some of the aircraft weight will be carried by the wings. This effect will tend to keep the footprint length constant. Since aerodynamic lift is proportional to the square of the velocity, the tire load during landing will increase rapidly to its equilibrium value as the aircraft decelerates. Therefore, during most of the braking roll, the footprint area and average contact pressure will remain fairly constant.

The contact pressure distribution will affect the local component of the friction force (i.e., the shear stress distribution). However, the observed friction and wear characteristics of a tire do not reflect the local components directly, but come from average values taken over the entire footprint. For example, the observed friction coefficient is, in effect, the average shear stress divided by the average contact pressure. This type of qualitative reasoning suggests that the friction and wear characteristics of a tire depend more on the average contact pressure than the pressure distribution. Therefore, the tests must simulate the average contact pressure closely. This can be done, for instance, by forcing the tread element with an air cylinder supplied from a constant-pressure reservoir. Subsequently, if needed, dynamic modulation of this pressure can be included.

(3) Tread Heating

Heating of the tread during braking has a strong influence on tire friction and wear. High temperatures, mainly caused by friction, can have two effects on the tread.

(1) Changes in the material properties (elasticity, friction coefficients, etc.) of the tread compound.

(2) Thermal degradation (reversion) of the rubber.

The present tread compounds for aircraft tires degrade at temperatures around 400 ~ 500° F (12). Such temperatures can be reached under severe loading conditions, such as locked wheel landings or hydroplaning. This type of operation leads to the formation of flat spots or patches of reverted rubber on the tread.

Even under normal conditions, instantaneous tread surface temperatures can reach several hundred degrees (° F). Here, tire friction and wear are affected due to changes in the material properties of the rubber. For instance, the friction coefficient[3] of

[3] Measured with the Drum apparatus.

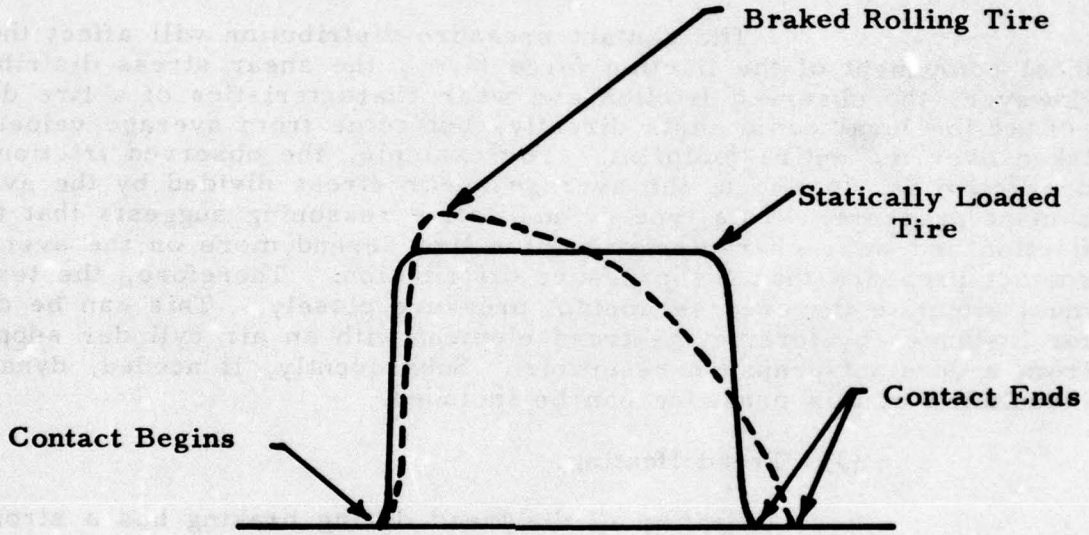

Figure 7 Contact Pressure Distribution for a Statically Loaded and Braked Tire

natural rubber decreases by about 40% with an increase in temperature from 60° F to 200° F (2). Present tread compounds are a mixture of natural and synthetic rubbers, and their material properties will also change significantly over the temperature range encountered in normal service.

The above discussion indicates why it is necessary to simulate the heating (and cooling) history of the tread element in order to obtain realistic results with the test machine. A sketch of the cyclic temperature variation of a tread element is shown in Figure 8. At A, the element enters the contact zone. For a short duration, its temperature drops due to heat transfer to the (cooler) pavement. At B, the element begins to slip and generate frictional heat. The slip increases towards the end of the contact zone, and the temperature rises sharply. At C, frictional heating has ended, and the element is at its highest temperature. During CD, the element moves through the air and dissipates heat by conduction (to the tire) and convection (to the surrounding air).

It is of interest to estimate the peak temperature rise of the tread surface to illustrate the importance of the various factors, such as tire velocity, slip, etc. The analysis of tread heat generation and transfer is a complex task. The combined effects of footprint pressure distribution, local friction coefficient variation, hysteretic heat generation and multidimensional, transient heat transfer make an exact analysis intractable. However, useful estimates of the maximum surface temperature rise can be obtained with the approximate analysis described in Reference (13). In this model, only frictional heat generation is considered, along with one-dimensional, transient heat conduction into the tread. For aircraft tires, these assumptions are reasonable, since during braking, hysteretic heating will be only a few percent of the frictional heat generation, and pavement cooling (AB) will be negligible. The temperature rise BC (Figure 8) is

$$\Delta T_{BC} \simeq (\mu ps/2\lambda)\sqrt{\frac{kLV}{\pi(1-s)}} \qquad (10)$$

where μ - friction coefficient

p - footprint pressure

s - slip

λ - thermal conductivity

k - thermal diffusivity

V - aircraft velocity

and L - footprint length.

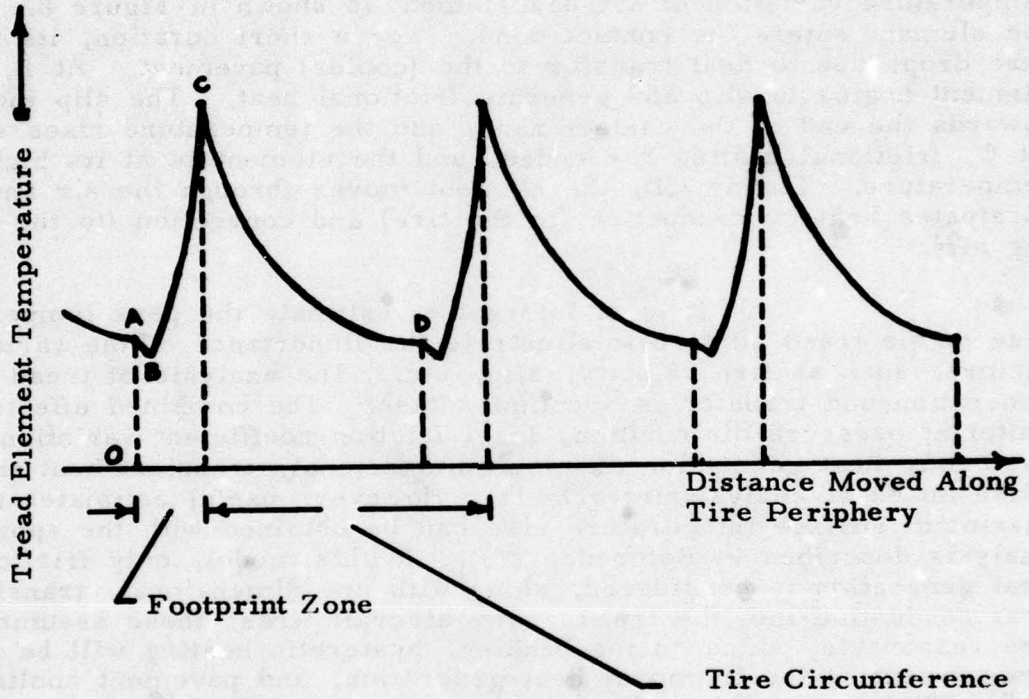

Figure 8 Temperature History of Tread Element

This result is shown in Figure 9 for a 20 x 4.4 tire. The parameters used for the calculation are given below

$\mu = 0.4$

$p = 234$ psi

$L = 8$ in

$\lambda = 5 \times 10^{-5}$ Btu/ft-sec-° F

$k = 2 \times 10^{-6}$ ft^2/sec

As expected, large temperature rises occur at high velocities and slips. In practice, this peak temperature rise along with ambient temperature effects will influence tire friction and wear. The above results are approximate, because, among other factors, they do not take the deformation slip into account. However, they indicate clearly, that significant variations in the material properties of the tread will occur. Since this will affect the friction and wear characteristics of the tire, the test machine must be designed to simulate the heating and cooling history of the tread element.

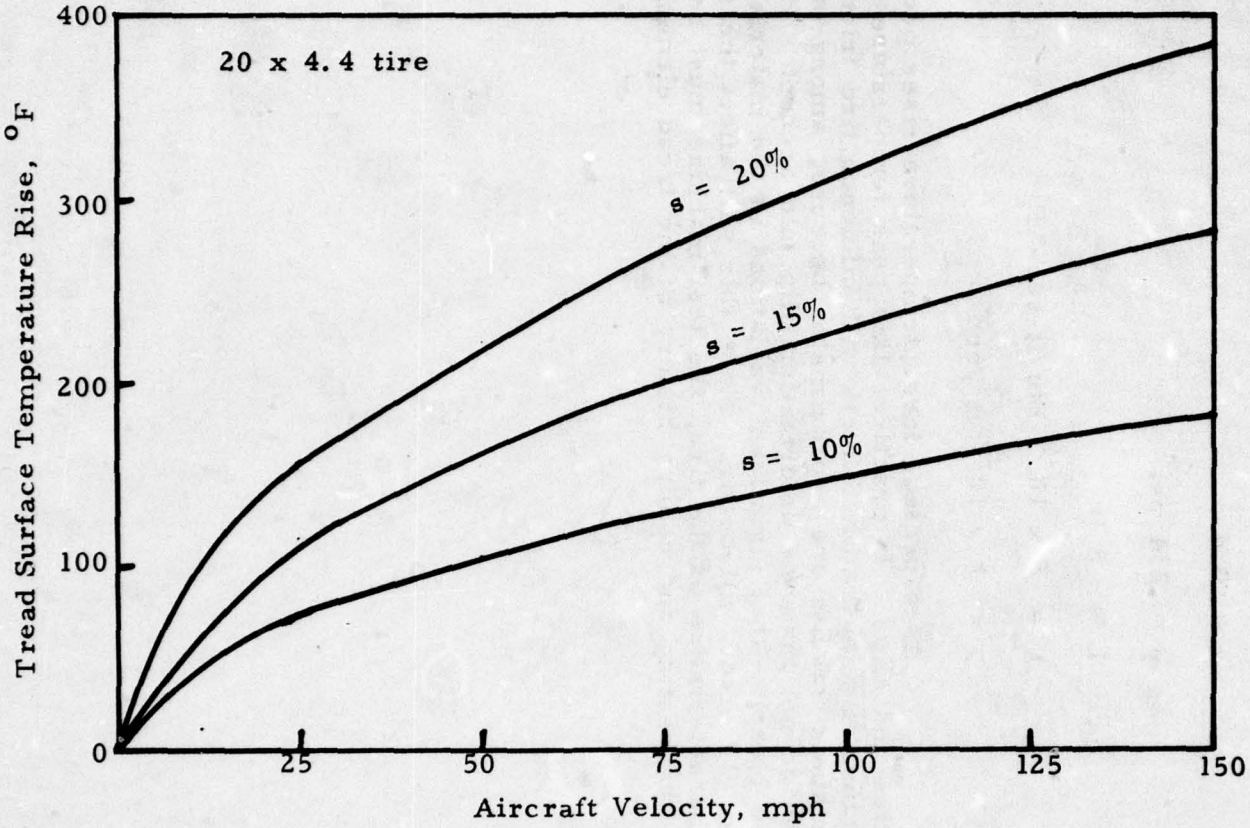

Figure 9 Tread Surface Temperature Rise Due to Frictional Heating

SECTION IV

DEVELOPMENT OF THE TEST METHOD

The preceding section has analyzed the forces, motions and heating for the tread during braking. These results are now used in selecting the simulation parameters and developing the test method. The basic procedure consists of simulating, for a tread element, those variables known to have a significant effect on tire friction and wear. This approach will reduce the initial cost and complexity of the machine while retaining sufficient capability for evaluating the main friction and wear characteristics of the tire. As development of the test method proceeds, the initial test results will be used to justify additional refinements for improving the simulation and studying other phenomena.

1. SELECTION OF SIMULATION PARAMETERS

The main parameters that affect tire friction and wear have been discussed in Section III. They are summarized in Figure 10. In general, friction and wear depend on the runway surface characteristics, the tread material properties and the loading. The dominant runway, tread and loading parameters to be simulated are discussed in the following paragraphs.

a. Runway Surface Characteristics

There are three runway characteristics that influence tire performance and should be simulated.

(1) Surface roughness

(2) Heat conductivity, and

(3) Water film thickness

The test pavement can be made from the same material as the runway, and dressed with an abrasive wheel, if necessary. This will minimize pavement contamination at the start of the test and provide a uniform surface that is comparable to that of a real runway.

The presence of a water film reduces considerably the friction coefficient available to decelerate the aircraft. The machine must have the capability to investigate this condition. A sprinkler system will be provided to establish the water film needed to simulate wet runway landing.

It is likely that the ambient temperature of the runway will not have a large effect on tire performance. Examination of Figure 8 shows that runway temperature only affects tire heating during portion AB of the contact zone. This is the entrance region at which the shear stress is small and relative movement has not begun.

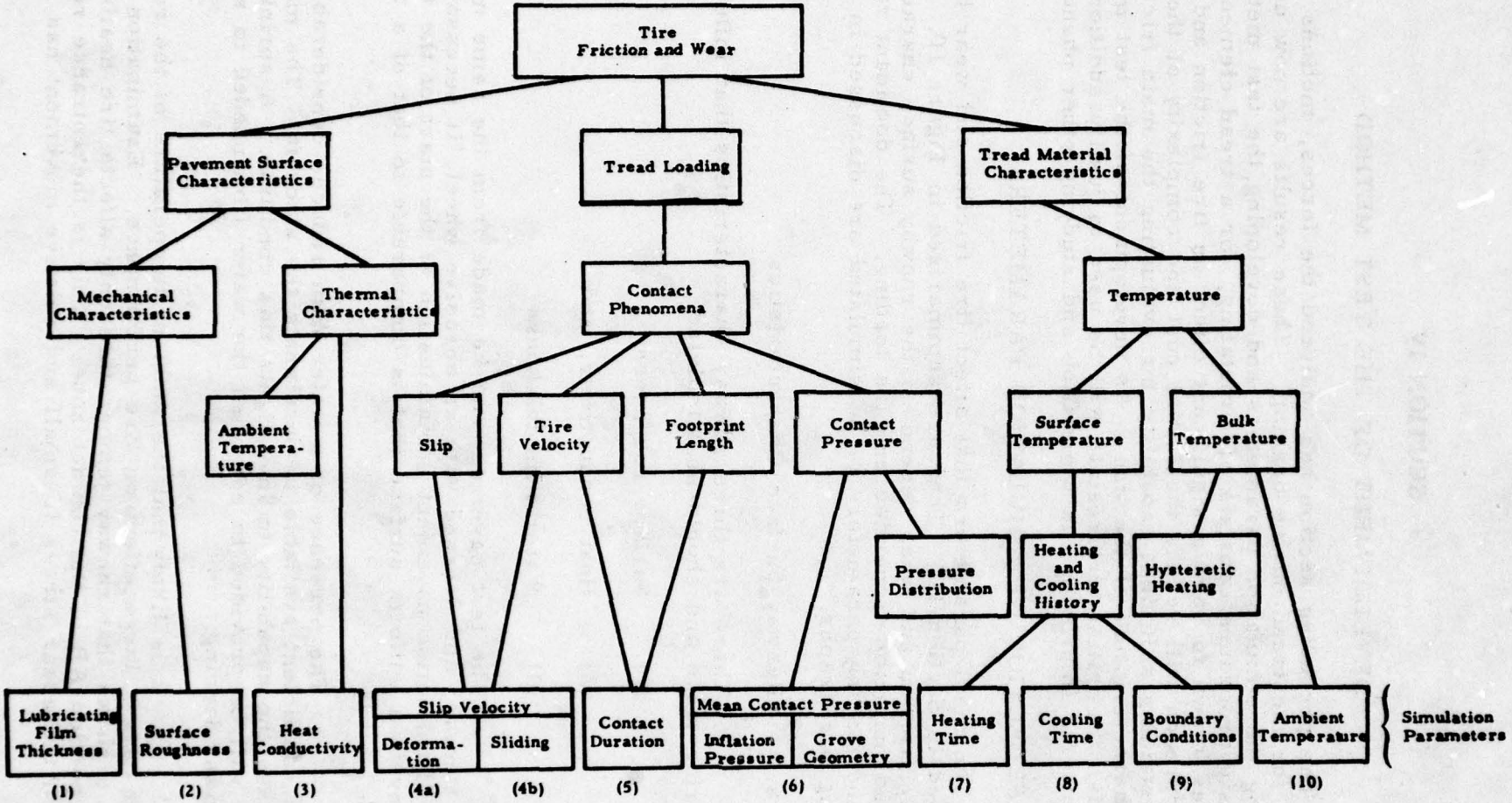

Figure 10 Principal Factors Affecting Friction and Wear in Aircraft Tires

Once frictional heating begins (BC), the interface temperature becomes so high that ambient runway temperature is insignificant in comparison. Under high braking slip, the duration of AB will be very small. Normal runway temperature variations will thus have only a secondary effect on tire performance, and simulation of this effect need not be included in the initial design.

b. Tread Material Properties

One of the advantages of this novel test method is that the tread element can be obtained directly from the tire under evaluation. This ensures that the compounding formula of the test specimen is the same as that of the tire. However, the material properties of rubber are temperature dependent. Thus, the bulk temperature of the test specimen must correspond to that of the tire tread. Also, the cyclic heating and cooling of the tread surface must also be simulated by the test.

The first of these can be done quite easily by heating (or cooling) the tread element until it reaches the required ambient temperature. Since the heating (or cooling) time constant of the tread element is much larger than the test duration,[4] the bulk temperature during the test will remain fairly constant, without the need for active temperature control. The change in bulk temperature due to hysteretic heating will be very small. The magnitude of this effect can be estimated by noting that, at small slip, most of the bulk temperature rise is due to hysteresis. Experiments with truck tires (12) at small slip show that equilibrium temperatures of $100 \sim 200\,^{\circ}F$ are reached after about 2 hours. Since a part of this temperature rise is certainly due to frictional heating, it would appear that the hysteretic temperature rise within the first two or three minutes will be of the order of a few degrees at most. Thus, for normal landings, lasting a minute or less, hysteretic heating will not significantly affect the bulk tire temperature and can be neglected.

The cyclic heating and cooling of the tire surface results in an unsteady temperature profile within the tread. The poor heat conduction characteristics of tread rubber cause high temperatures and large temperature gradients to be established. These effects are confined to a thin surface layer which is on the order of 0.01 in. for common tread materials (13). The rate of heat generation due to frictional heating depends primarily on the contact pressure, tire velocity and slip. In order to approximate the tread surface temperatures as closely as possible, it is necessary to simulate these variables and to carry out the testing in real time. Although there is no friction or wear when the tread is not in contact with the pavement, there is surface cooling by conduction and convection. The peak tread temperature depends on the available cooling time, so that the cooling effect must be simulated during the tests. It is also desirable to duplicate

[4] See Section V.

the thermal boundary conditions as closely as practical. For instance, the width of the tread element can be kept equal to the width between grooves, thereby retaining the natural lateral boundary for convection.

In summary, the four parameters that establish temperature correlation between the test specimen and the tire tread are listed below.

(1) Ambient temperature of tread element

(2) Thermal boundary conditions

(3) Frictional heating time

(4) Cooling time

These must be simulated, so that the material properties of the tread element correspond to those of the tire under evaluation.

c. Tread Loading

There are three loading parameters to be simulated:

(1) Contact pressure

(2) Contact duration, and

(3) Slip

A tread element of a braked tire will be stressed cyclically as it passes through the contact zone. In this region, it will have a very complex state of stress. However, the primary stresses will be due to the contact pressure and the friction force. The latter will depend on the contact pressure, the runway surface characteristics, the tread material properties and the temperature. The temperature in the contact zone will be largely dependent on the frictional heating caused by slip. The wear rate will also depend on the contact pressure and slip. Thus, the tire loading parameters to be simulated are contact pressure, contact duration and slip. As discussed in Section III, the observed slip has two components -- one caused by tread elasticity and the other by sliding. These can be simulated by duplicating, as far as practical, the boundary conditions for the tread element, as will be described in Section V. Although the pressure within the footprint is not uniform, observed tire friction and wear are average values which depend primarily on the mean contact pressure. Simulation of this pressure is essential. The test method can later be refined to simulate a nonuniform pressure distribution if indicated by the initial test results.

2. TEST PROCEDURE

The test procedure consists of:

a. Programming the controller

b. Initiating the sequence, and

c. Evaluating the data

These operations are described below.

a. Programming of Test Controller

The test controller automatically controls the input parameters needed to simulate a specified landing. There are four such parameters to be controlled. These are

(1) The slip velocity

(2) The runway contact frequency

(3) The contact time, and

(4) The cooling time

The slip velocity V_s is

$$V_s = sV \tag{11}$$

where s is the slip

and V is the aircraft velocity.

The ratio of the cooling time to the contact time T_{cool}/T_{cont} is

$$T_{cool}/T_{cont} = \pi D/L - 1 \tag{12}$$

where πD is the tire periphery

and L is the footprint length.

For most tires, the contact ratio $\pi D/L$ is fairly constant and approximately equal to 7 (see Table III). Thus,

$$T_{cool} \simeq 6\, T_{cont} \tag{13}$$

The contact frequency f_c is

$$f_c = 1/(T_{cont} + T_{cool}) = (1 - s)\, V/\pi D \tag{14}$$

where s is the slip,

V is the aircraft velocity

and D is the tire diameter

From Equations (12) and (13), it can be seen that the contact frequency and the cooling and contact duration depend only on the ratio $(1-s)V/\pi D$.

The four simulation parameters mentioned earlier can be controlled by specifying, as functions of time, just two variables, namely V_s and f_c. It is therefore necessary to program only these variables to simulate any specific landing.

Both V_s and f_c will change during landing. Before the wheel brakes are applied, V_s will be practically zero, and need not be simulated. The test should commence after braking begins. The general nature of the variation of V_s and f_c is shown in Figure 11a. Exact curves for any specific landing can be calculated from Equations (11) and (14). The slip velocity and contact frequency at the start of the test are high, in order to simulate a fast rolling tire. As the aircraft decelerates, these variables decrease. The test terminates at the point where the wheel brakes are released.

b. Initiation of Test Sequence

Once the slip velocity and contact frequency have been programmed, the test can begin. The following operations must be carried out to initiate the test sequence.

(1) Heating or cooling of tread element to the desired bulk temperature, and attachment to the loading mechanism.

(2) Reset of loading mechanism to deliver appropriate contact force.

(3) Activation of measurement system and pavement and loading drives.

(4) Start of water sprinkler (if needed), and

(5) Transfer of control to programmer.

From this point on, the test will proceed automatically, and the data will be recorded for subsequent evaluation.

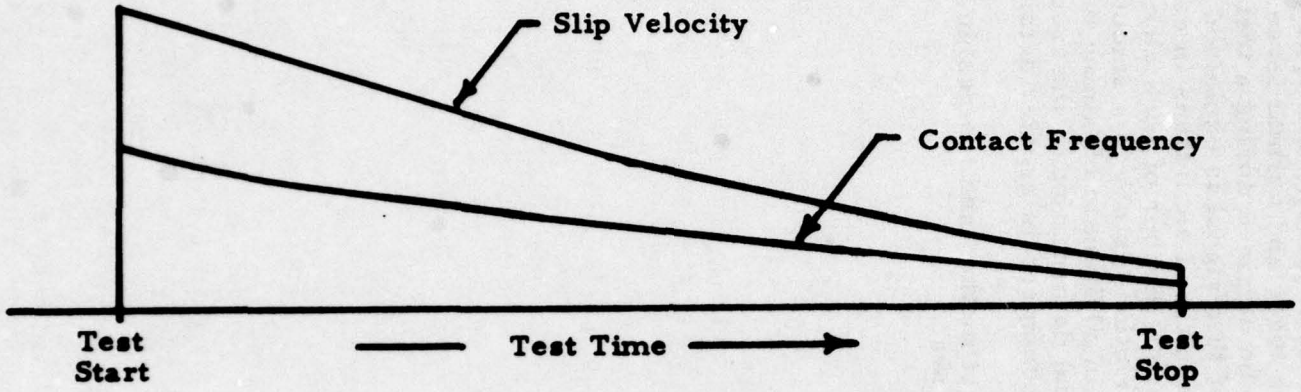

(a) Programmed Input Variables

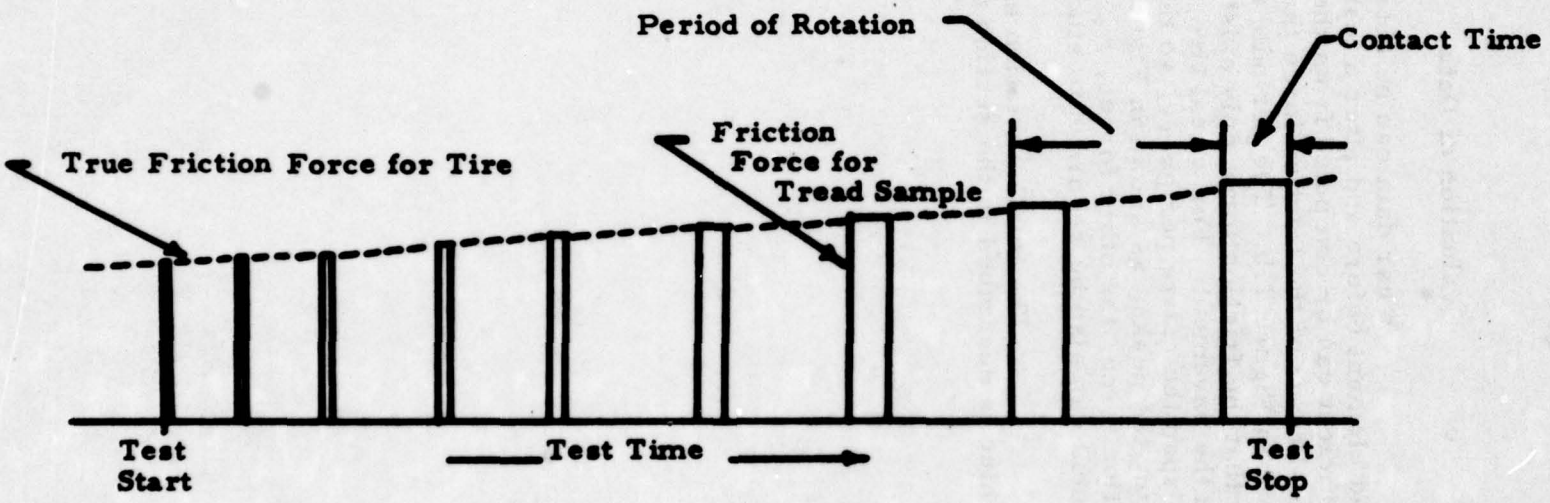

(b) Output Data for Friction Force

Figure 11 Programmed Input Variables and Output Data

c. Evaluation of Data

Wear data can be obtained most accurately by weighing the tread element before and after a test (or series of tests). The friction coefficient can be computed from the friction force and normal force. A typical trace of the friction force that would be obtained during a test is shown in Figure 11b. The periodic nature of this signal is explained by the fact that the friction force only exists when the tread element is in contact with the pavement. For a real tire, there are a number of such elements that span the entire periphery, so the true friction history is a smooth curve joining the peaks, as shown in Figure 11b. In addition to obtaining the friction force, the other forces, moments and deformation of the tread element can also be recorded to study the phenomena in greater detail.

The implementation of this test method and the design of the machine is described in the section that follows.

SECTION V

DESIGN OF THE PROTOTYPE MACHINE

A prototype machine has been designed to implement the test method developed in the previous section. The machine concept was described in Section I. The functions of the individual subsystems are summarized in Table IV. Each function is referenced to show the way in which it is related to the simulation parameters described in Figure 10. The hardware for these subsystems has been designed, and engineering drawings and/or specifications for the components and assembly have been prepared. The following sections describe the layout and the important features of the subsystems, and present the supporting design calculations.

1. THE TREAD ELEMENT

The test sample is obtained by removing a small tread element from the tire under evaluation (see Figure 12). In a properly inflated tire, most of the wear occurs at the crown. To give representative results, the tread element should be obtained from this region, preferably near the center. The size of the element is important. A small sample will give results that are strongly affected by end conditions which do not exist in the tire. A large sample will increase the curvature of the element and will require more power to run the test. An acceptable tradeoff is to select a sample that is large enough to be tested conveniently but small compared to the tire footprint.

a. Configuration

The shape of the tread element must be chosen such that the mechanical and thermal boundary conditions conform, where practical, to those of the loaded tire. The walls of the tread grooves form the lateral boundaries for convective heat transfer and are free of normal stress. Therefore, a logical choice is to keep the width of the tread element equal to the width between grooves. For large tires, the element can be cut from the region between adjacent grooves. For smaller tires, the tests can be conducted with two or three different sample sizes. The friction and wear per unit area can be compared to indicate the severity of extraneous edge effects and provide guidelines for future improvements.

On a microscopic scale, different regions within the contact zone have different values of slip. The shear stresses and strains will also be different. This condition can be approximated by allowing the shear strains to take place over an element thickness equal to the tread thickness. This means that the height of the test sample must be equal to the thickness of the tire crossection at the crown.

The tread element should be long enough to inhibit buckling or squirming under the combined action of the compressive pressure and the lateral force. A length equal to twice the height should be adequate. This can be checked during the initial tests and modified if needed. Data obtained with elements of different sizes, will show the influence of the shape parameters

Table IV Description of Machine Subsystems

Subsystem	Controlled Variable	Function
1. Tread Element	Shape and compliance	Simulation of sliding and deformation slip components and heat boundary conditions (4a, 4b, 9).
	Bulk temperature	Simulation of ambient temperature property changes of tread (10).
2. Pavement Drive	Table speed	Simulation of gross slip of tread (4).
3. Pavement Table	Material characteristics	Simulation of runway roughness and heat conductivity (2, 3).
	Loading force	Simulation of average footprint pressure (6).
4. Loading Mechanism	Load duration	Simulation of contact time and heating time for tread element (5, 7).
	Loading frequency	Simulation of cooling time for tread element (8).
5. Sprinkler	Water flow	Simulation of lubricating film characteristics (1).
6. Decontamination	---	Removal of abraded rubber from pavement.
7. Test Controller	---	Automatic test control by programming landing speed history, slip, inflation pressure and tire size parameters.
8. Instrumentation and Recording	---	Measurement of the friction force and the other forces, moments and deflection of tread element.

(Numbers in parentheses refer to parameters identified in Figure 10)

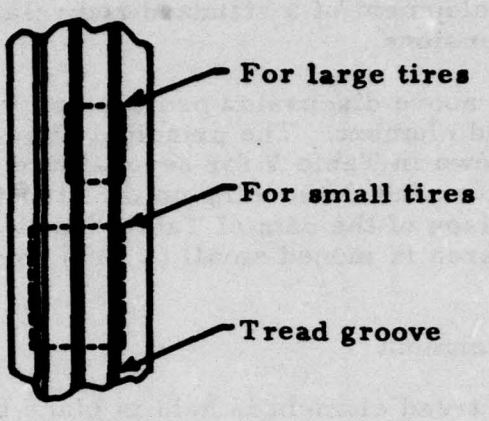

(a) Removal of Tread Element

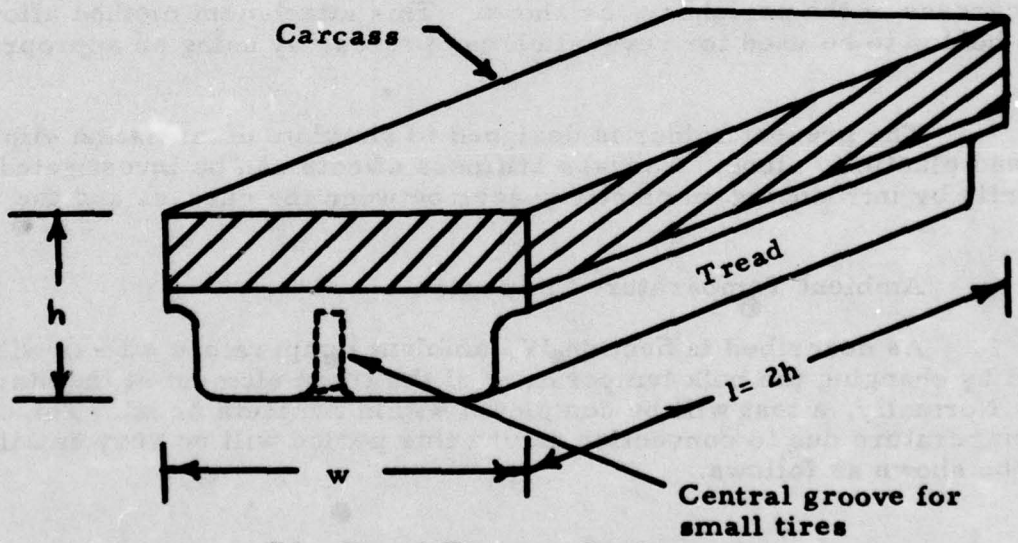

(b) Tread Element Configuration

Figure 12 The Tread Element

and lead to the development of a standardized relationship for calculating tread element dimensions.

The above discussion provides an initial basis for determining the size of the tread element. The principal dimensions and normal force on the element are shown in Table V for several tire sizes. This information is used later to determine the loading on the structural members of the machine. Comparison of the data of Table V with that of Table II shows that the tread element area is indeed small (< 10%) compared to the tire footprint.

b. Attachment

The tread element is held in place by a holder which is fastened to the machine. During the early part of the landing simulation, the holder will force the tread against the pavement at a very high frequency -- up to about 40 hz for the smaller tires. For this reason, the weight of the holder must be minimized to limit the inertia force. Two holders have been designed. A small light holder of welded construction for the smallest tires such as the 20x4.4 and the 30x8.8. The weight of this holder (with tread element) is estimated to be 1.8 lbs. For the larger tires, such as the 49x17 and the 44x16, where the frequency is lower, but the loading is high, a stronger holder has been designed. This holder (with tread) will weigh about 5 lbs. A drawing of the holder-tread assembly is shown in Figure 13.

Initially, the tread element is obtained from the tire and cut to size. The peripheral tread is stripped away to expose the carcass. It is then glued to a backing plate for rigidity and fastened to the holder by clamping the exposed carcass at the periphery, as shown. This attachment method allows the same holder to be used for several element sizes, by using an appropriate clamp.

The present holder is designed to simulate deformation slip[5] due to tread elasticity alone. Carcass stiffness effects can be investigated subsequently by introducing an elastic spacer between the carcass and the clamp.

c. Ambient Temperature Simulation

As described in Section IV, ambient temperature effects will be simulated by changing the bulk temperature of the tread element at the start of the test. Normally, a test will be completed within a minute or so. The change in bulk temperature due to convection during this period will be very small. This can be shown as follows.

[5] See Section III.

Table V Typical Tread Element Dimensions

Tire Size	Tread Element Dimensions				Contact Parameters	
	h (in)	l (in)	w (in)	Area (in^2)	Normal Force (lbs)	Normal Deflection (in)
56x16	1.56	3.12	3.5	10.9	3,580	0.15
49x17	1.25	2.5	3.37	8.44	1,490	0.075
44x16	1.26	2.52	3.25	8.2	1,710	0.082
36x11	1.1	2.2	1.31	2.89	705	0.093
30x11.5-14.5	1.25	2.5	2	5	1,275	0.137
20x4.4	0.82	1.64	1.125	1.85	432	0.074

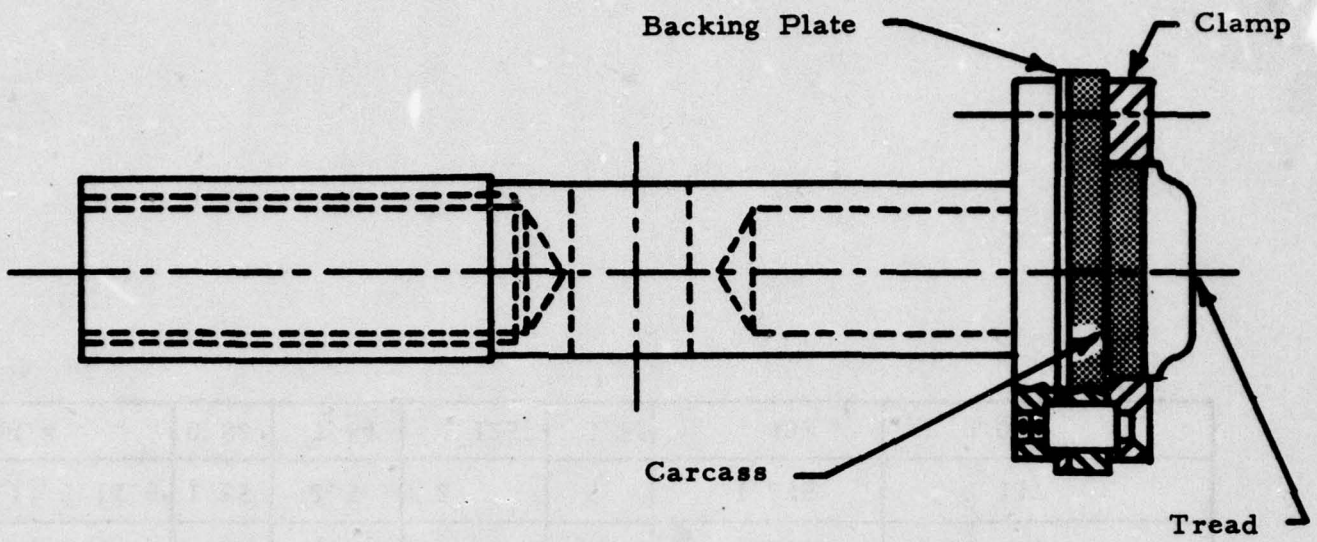

(a) Small Tires

Figure 13 Attachment of Tread Element

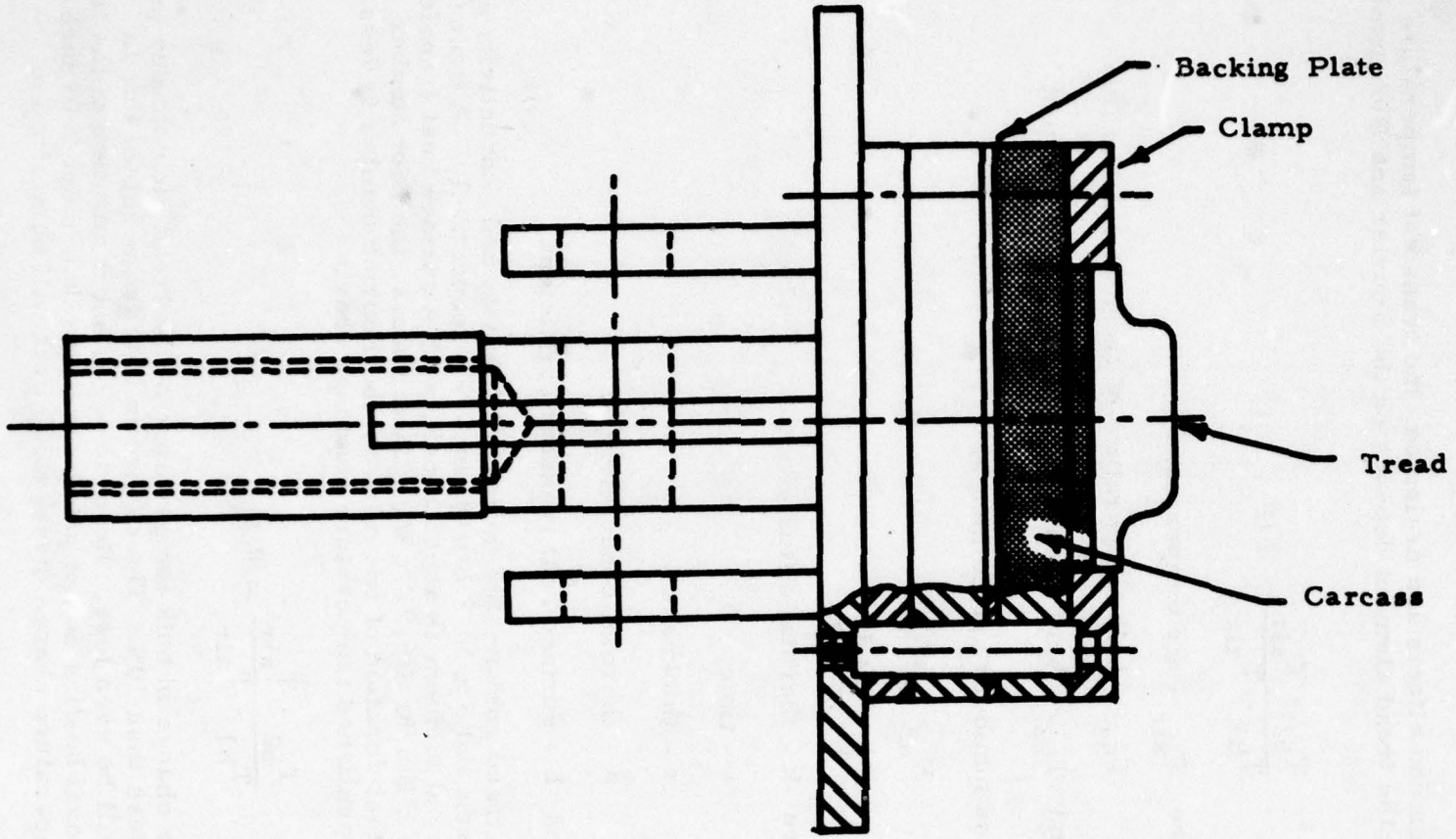

(b) Large Tires

Figure 13 --- Concluded

When end effects are neglected, the transient temperature distribution within the tread element depends on the Fourier and Biot numbers (14)

$$\frac{T_{b2} - T_{air}}{T_{b1} - T_{air}} = f(F_o, B_i) \tag{15}$$

where T_{air} - air temperature

T_{b1} - bulk temperature of tread at start of test

and T_{b2} - bulk temperature of tread at end of test.

These numbers are defined as

$$F_o = 4kt/r^2 \tag{16}$$

$$B_i = 2\lambda/hr \tag{17}$$

where k - thermal diffusivity

t - time

r - thickness

λ - thermal conductivity

and h - surface heat transfer coefficient.

For tread rubber, the thermal diffusivity and conductivity are about 2×10^{-6} ft^2/sec and 5×10^{-5} Btu/ft-sec-^oF, respectively. A typical thickness for the tread element is about 1 inch, with a surface heat transfer coefficient of about 2 Btu/hr-ft^2-^oF. With these values, the Biot number is about 2. For a test duration of one minute, the Fourier number is less than 0.1. Referring to published temperature response charts (14).

$$\frac{T_{b2} - T_{air}}{T_{b1} - T_{air}} \simeq 0.9 \tag{18}$$

This means that the change in bulk temperature of the tread element due to convection will be less than 10%. The change in bulk temperature due to frictional heating will be even less. Because of the short duration of the test, the effects of frictional heating do not penetrate more than about 0.01 inch (13). The bulk temperature change due to this effect will be negligible.

Since the bulk temperature of the tread element remains fairly constant during a test, there is no need for an active temperature control system. This results in a simpler machine and reduces the fabrication cost.

The actual heating or cooling of the tread prior to the test can be carried out in three ways.

(1) Heating/cooling the tread element in an environmental chamber, and attaching it to the holder after the desired temperature has been reached.

(2) Heating/cooling the tread element and holder assembly and attaching it to the machine as a unit after the desired temperature has been reached.

(3) Attaching the tread to the machine and heating/cooling it by means of conduction from an external hot/cold plate pressed against the tread surface.

The choice from among these options will depend on the equipment available and the attachment time for the tread and the holder. The initial test results will indicate which of the above three methods is the most convenient and effective.

2. THE PAVEMENT TABLE

The pavement table consists of an annular section of concrete or asphalt fastened to a circular base. A sketch of the assembly is shown in Figure 14. It consists of three principal parts, the pavement, the holder and the flywheel.

The pavement is cast directly into the pavement holder. This eliminates the need for additional molds or fasteners. After being cast, the pavement surface can be dressed with an abrasive wheel to the desired degree of roughness. For the initial tests, two interchangeable pavement holders have been provided. One of these will contain a concrete pavement and the other will contain asphalt. If needed subsequently, additional holders can be fabricated. The pavement-holder assembly can be changed by removing the bolts that fasten the holder to the base.

When the tread element is in contact with the rotating (annular) pavement, there will be a difference in the slip velocity across the element width. This lateral variation does not occur during the straight-line motion of a tire. Therefore, it is desirable to keep the lateral variation small compared with the peripheral velocity. This condition implies that there is a tradeoff between the size of the table and the variation in lateral velocity. Most tread elements are about $1 \sim 3$ inches in width. An effective pavement diameter of 3 ft. will result in lateral variations that are within about $3 \sim 10\%$ of the mean velocity, depending on the tire size.

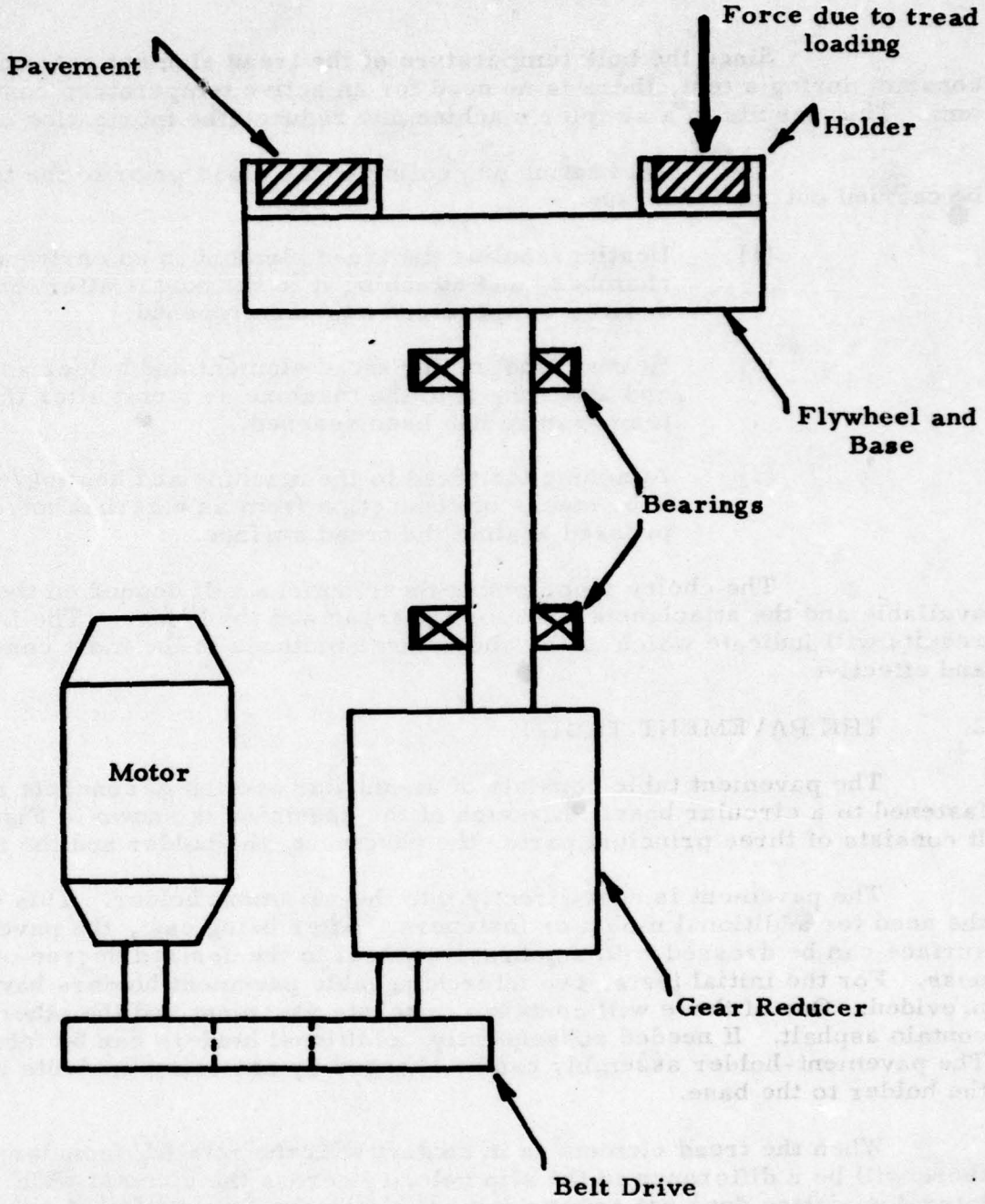

Figure 14 Configuration of Pavement Table and Drive System

The base transmits the contact force from the tread element to the bearings. It also acts as a flywheel to reduce speed fluctuations of the pavement drive system. The flywheel dimensions have been chosen such that the moment of inertia of the pavement table is about 80 lb-ft-sec^2. The weight will be about 2000 lbs. The former estimate is used in performing the dynamic analysis of the pavement drive system described later.

As discussed in Section IV, runway temperature variations will have only a secondary effect on tire performances. Therefore, no pavement temperature control system has been provided for the prototype machine. Subsequently, if pavement temperature effects are to be studied, a pavement heating (cooling) system can be added. High pavement loads and poor thermal conductivity will make it unattractive to heat (cool) the pavement with subsurface heating (cooling) coils. A more favorable scheme will be to preheat (pre-cool) the pavement prior to the test, and control its temperature during the test by convective heating (cooling) with a jet of hot (cold) air.

3. PAVEMENT DRIVE

The pavement drive system turns the pavement table and establishes the slip between the pavement and the tread element. The layout of this system is shown in Figure 14.

For precise speed control, a variable speed, regenerative, DC motor drive (1750 rpm) has been chosen to power the system. The power is transmitted to the pavement table through a timing belt drive and a gear reducer. The peripheral velocity of the pavement must correspond to the slip velocity of the tire. The table rpm is

$$N = \frac{60\, s V_a}{\pi D} \tag{19}$$

where N - pavement table rpm

s - fractional slip

V_a - aircraft velocity (ft/sec)

and D - effective pavement diameter (ft).

The touchdown velocities of most operational aircraft lie between 110 ~ 160 knots. Although the wheel brakes will be applied at a lower speed, conservative design calculations can be based on these touchdown speeds. For a braking slip of 15 ~ 20%, Equation (19) gives a maximum table speed of 200 ~ 350 rpm for the proposed table dimensions. A 6.2:1 gear reducer decreases the (nominal) maximum motor speed from 1750 rpm to 280 rpm. This nominal rating of the motor is adjustable within ± 25%, so that the maximum table speed for most tests can be obtained with a fixed ratio speed reducer. However, for cases where the landing speed or slip is outside the range considered, provision is made to obtain the appropriate table speed

by changing the pulleys on the belt drive. The design calculations for selecting the bearings, the motor and the gear reducer are summarized below.

a. Bearings

The loading diagram for the bearings and the bearing reactions are shown in Figure 15. The forces indicated represent the most severe case of loading, which occurs when evaluating the 56x16 tire at a friction coefficient of unity. In practice, these forces will be less, so that the design calculations presented here are conservative.

For the forward bearing,

$$F_{r1} = 4500 \text{ lbs.}$$

$$F_{a1} = 0 \text{ lbs.}$$

$$N = 350 \text{ rpm}$$

and for the rear bearing

$$F_{r2} = 3300 \text{ lbs.}$$

$$F_{a2} = 4000 \text{ lbs.}$$

$$N = 350 \text{ rpm}$$

where F_r is the radial force

F_a is the axial force

and N is the bearing speed.

The bearings have been selected after consultation with the manufacturer, SKF Industries, Inc., Philadelphia, Pennsylvania. For the bearings selected (No. 22236C in front and No. 22232C in the rear), the rated life under the above loading conditions is in excess of 300,000 hours (15). Since the bearing speed is low and the machine will operate intermittently, grease lubrication can be used. Lubrication ports have been provided for this purpose.

b. Drive Motor

Selection of the pavement drive motor depends on the loading history and the inertia of the drive train. An equivalent diagram, showing the inertia of the principal components, is sketched in Figure 16.

The motor specifications are determined for the 56x16 tire, since this represents the most severe loading condition.

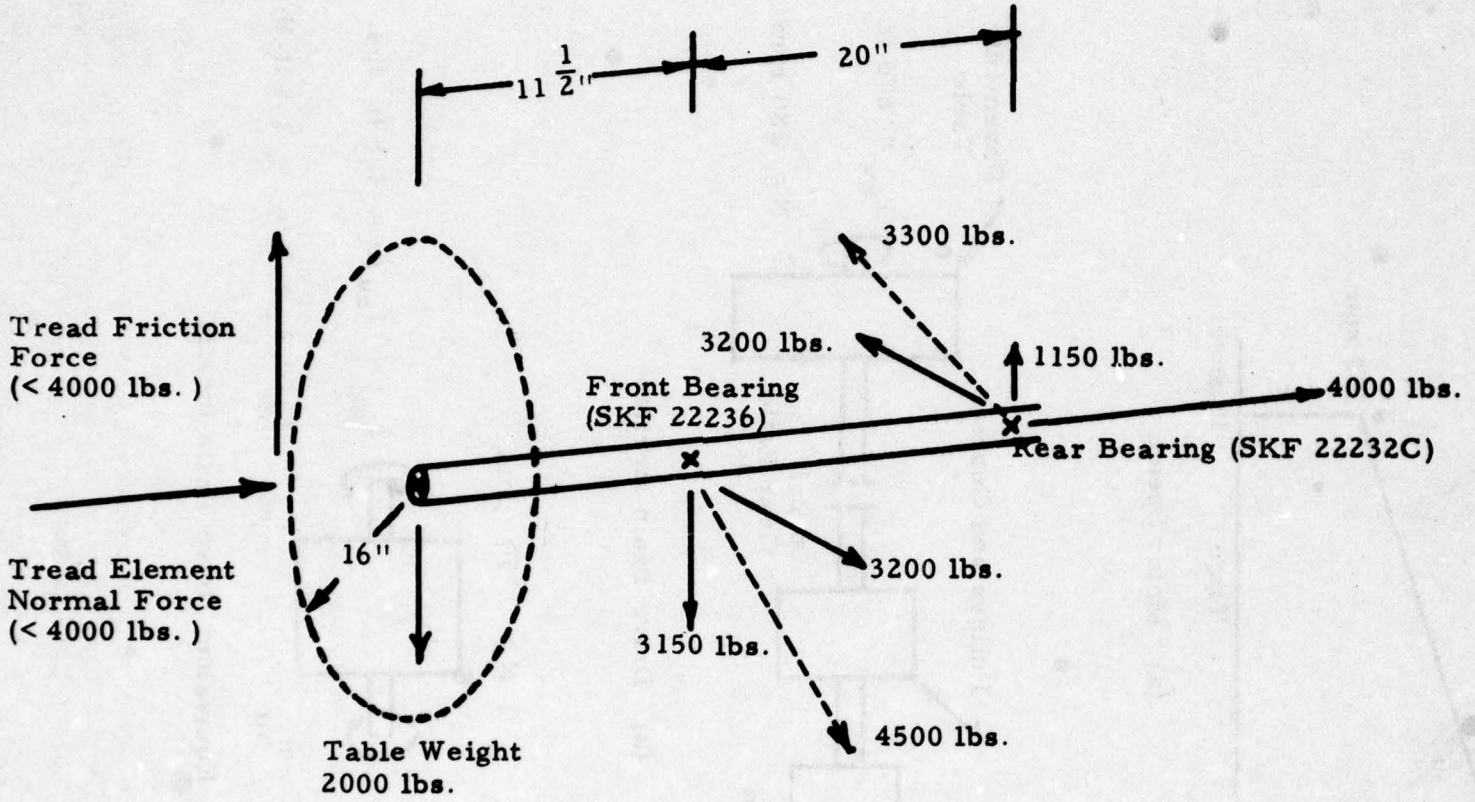

Figure 15 Loading Diagram for Pavement Table Bearings

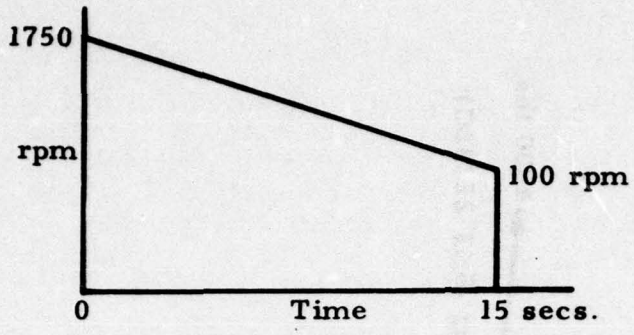

(a) Motor Speed

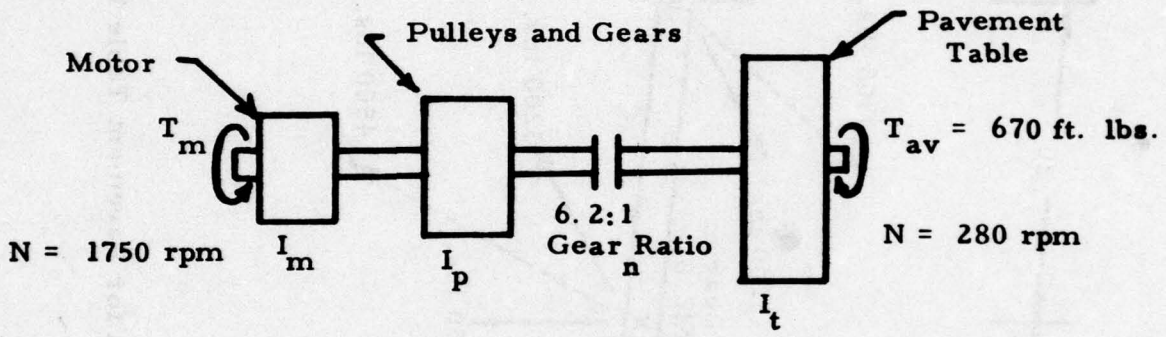

(b) Drive Train Inertias

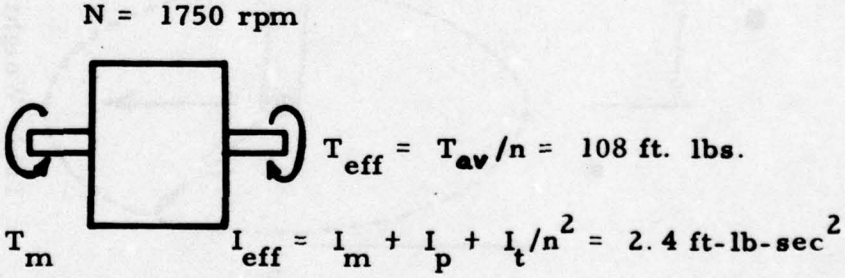

(c) Equivalent Drive Train Inertia

Figure 16 Drive Train Loading and Inertia Diagrams

The normal load on the tread element of this tire is 3500 lbs. For a maximum expected friction coefficient of unity, the friction force is equal to the normal load. The friction torque on the pavement spindle is 3500x16 = 56,000 in lbs. This torque acts cyclically to simulate periodic contact between the ground and a particular point on the tire. The average value of the friction torque is

$$T_{av} = T_{max}/C.R. \tag{20}$$

where C.R. is the contact ratio, i.e., tire circumference divided by footprint length.

With a contact ratio of 7 (see Table III), the average friction torque is 670 ft. lbs. The drive train inertias are as follows.

Table Inertia, $I_t = 80$ lb-ft-sec^2.

Pulley and Gear Inertia $I_p = 0.2$ lb-ft-sec^2.

Motor Inertia $I_m = 0.12$ lb-ft-sec^2.

These parameters are indicated in Figure 16b. The pavement spindle and motor shaft operate at different speeds, as shown. Reflecting all the inertias and torques to the motor shaft, an equivalent loading diagram can be drawn as shown in Figure 16c.

For equilibrium, the motor torque must equal the sum of the applied torque and the inertia torque

$$T_m = T_{eff} + I_{eff} d^2\theta/dt^2 \tag{21}$$

During the test, the pavement will decelerate, to simulate aircraft deceleration during braking. The actual speed-time relationship will depend on the aircraft and the environment, but for design calculations, a constant deceleration can be assumed. The resulting speed-time curve for the motor during a typical simulated landing is sketched in Figure 16a. The motor deceleration is about 11.5 rad/sec^2. Substituting the appropriate values into Equation (21)

$$T_m = 80.4 \text{ ft-lbs.}$$

The motor power is

$$P = \frac{2\pi NT}{33000} = \frac{2\pi x1750x80.4}{33000} \simeq 27 \text{ hp}$$

The motor to be selected must have a rating higher than the above figure. A 40 hp motor has been specified. This rating is adequate for all of the tests that are presently envisioned, and it will also provide a large reserve capacity which may be needed to implement future modifications.

Technical and cost data on the motor were solicited from three manufacturers. A tentative selection of the Westinghouse 40 hp 1750 rpm regenerative dc drive has been made. This type of motor has excellent speed control characteristics, and can be programmed to accelerate or decelerate precisely according to an input voltage command. A final selection of the motor will be made after fabrication of the machine is authorized, and the manufacturers technical and cost information reconfirmed.

The periodic loading of tread will result in fluctuations in the pavement table speed. At the start of the test, the loading frequency will be high, and the motor will be unable to respond. For this condition, the torque fluctuations will be counteracted by changes in the flywheel kinetic energy. The speed variation per cycle will be

$$\frac{\Delta \omega}{\omega} = \frac{\Delta Tt}{I\omega} \qquad (22)$$

where $\Delta \omega$ - speed change

ω - motor speed

ΔT - torque fluctuation

I - flywheel inertia

and t - contact time.

Evaluating this expression for the test of a 56x16 tire, the speed fluction at the start of the simulation will be about 1-1/2%. At lower speeds (during the end of the test), torque fluctuations will be counteracted by changes in the motor torque.

c. Gear Reducer

A 6.2:1 gear reducer is used to reduce the motor speed. The torque at the pavement spindle will be fairly constant, because there is a flywheel that will counteract the dynamic torque variations. The gear reducer power rating can thus be similar to that of the motor, i.e., 40 hp. Since the output shaft speed is 280 rpm, the torque is

$$\frac{40 \times 33000}{2\pi \times 280} = 750 \text{ lbs-ft.}$$

A Litton 6.2:1 gear reducer rated for an input speed of 1750 rpm and an output torque of 1700 lbs-ft has been chosen. Here again, a large reserve capacity is provided in case it is needed to implement future modifications.

4. LOADING MECHANISM

The loading mechanism forces the tread element cyclically against the rotating pavement table. The pavement contact time equals the time required by the element to move through the tire footprint. This increases throughout the landing simulation to represent the case of a decelerating tire. The frequency of contact depends on the tire size, rpm and slip. The most severe loading condition for the machine will occur during the initial (high-speed) part of the simulation, when the contact time is small and the contact frequency high. A bound for these parameters is given in Table III for several tire sizes and landing speeds. In practice, these values are conservative because the brakes-on speed will be lower than the touchdown velocity, and braking slip will further reduce tire rpm (and increase the element contact time). The design however has been carried out for the extreme conditions of touchdown velocity to provide a margin for future contingencies.

Figure 17 shows the tread element force and displacement history to be established by the machine. Two mechanisms capable of providing this motion were evaluated -- a slider-crank linkage and a cam-follower mechanism. The conventional slider-crank mechanism was found unsuitable, because the tread motion requirements could only be obtained with an unusually short connecting rod. The resulting angular excursions were very large, which led to unacceptably high forces in several of the key structural elements. Compound cranks were eliminated because of their great mechanical complexity.

A cam and follower mechanism was selected for the prototype design. This type of arrangement, under roughly similar loading conditions, has been used successfully in the past, in textile machinery. Communications with a cam manufacturer (16) have indicated that the contact stresses at the cam-follower interface are acceptable, but the follower (not the cam) may require occasional replacement due to brinelling.

A simplified diagram of the loading mechanism is shown in Figure 18. A pair of cams and followers advance and retract the tread element. A constant pressure air cylinder is provided to maintain a constant load on the element while it is in contact with the pavement. The retraction force for the tread is transmitted through an elastic stop. The contact force can be selected prior to the test, by adjusting the regulator that controls the inlet pressure to the air cylinder. The cams are driven by a variable speed regenerative dc motor drive. The camshaft speed determines the contact time and frequency. The principal design considerations for the cams and followers and the drive are described below.

a. Cams and Followers

A sketch of the follower motion during one rotation of the cam is shown in Figure 19. The loading on the cams and followers will be caused by inertia forces and the normal force of the tread element during contact. Referring to Figure 19, during the motion (1-2) and (3-4), the followers will be moving at constant velocity, so there will be no inertia load. Since the element

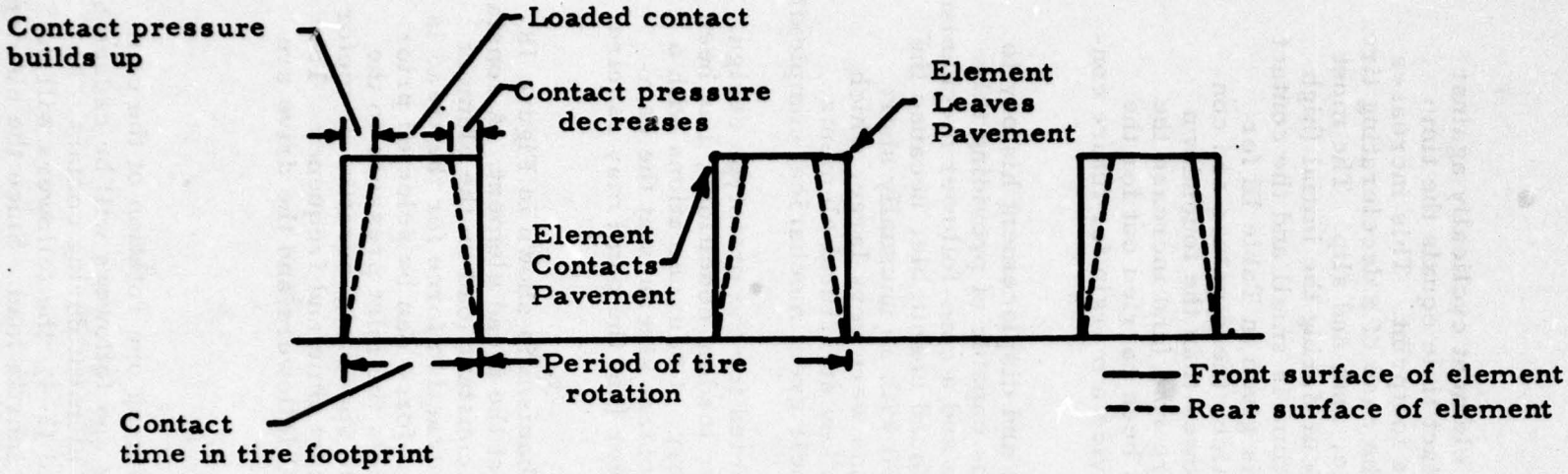

(a) Motion of Tread Element*

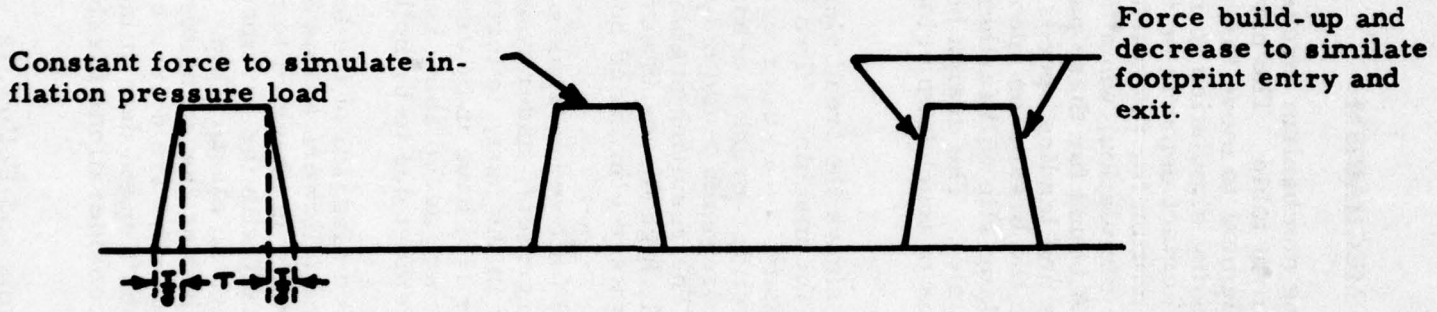

(b) Force Variation*

Figure 17 Force and Displacement History for Tread Element

*Diagrams are shown exagerated for clarity.

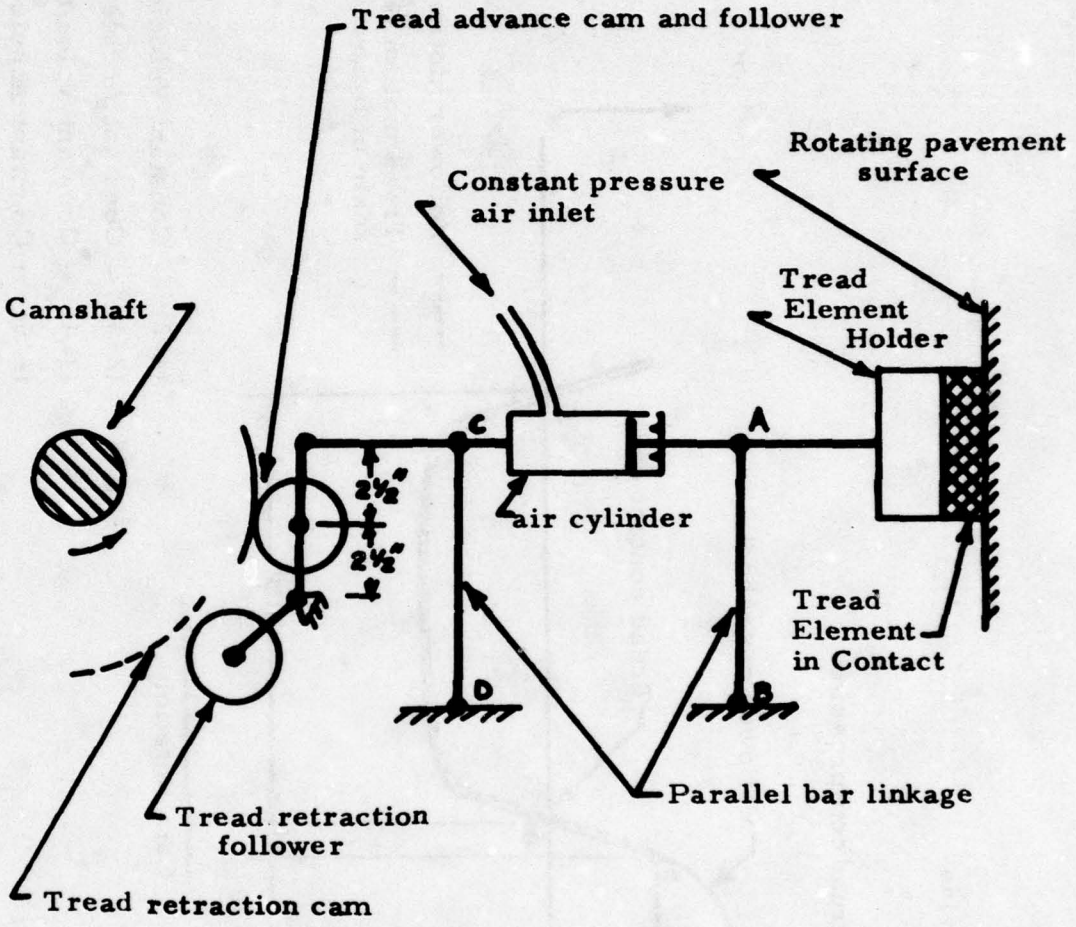

Figure 18 Schematic Diagram of Tread Loading Mechanism

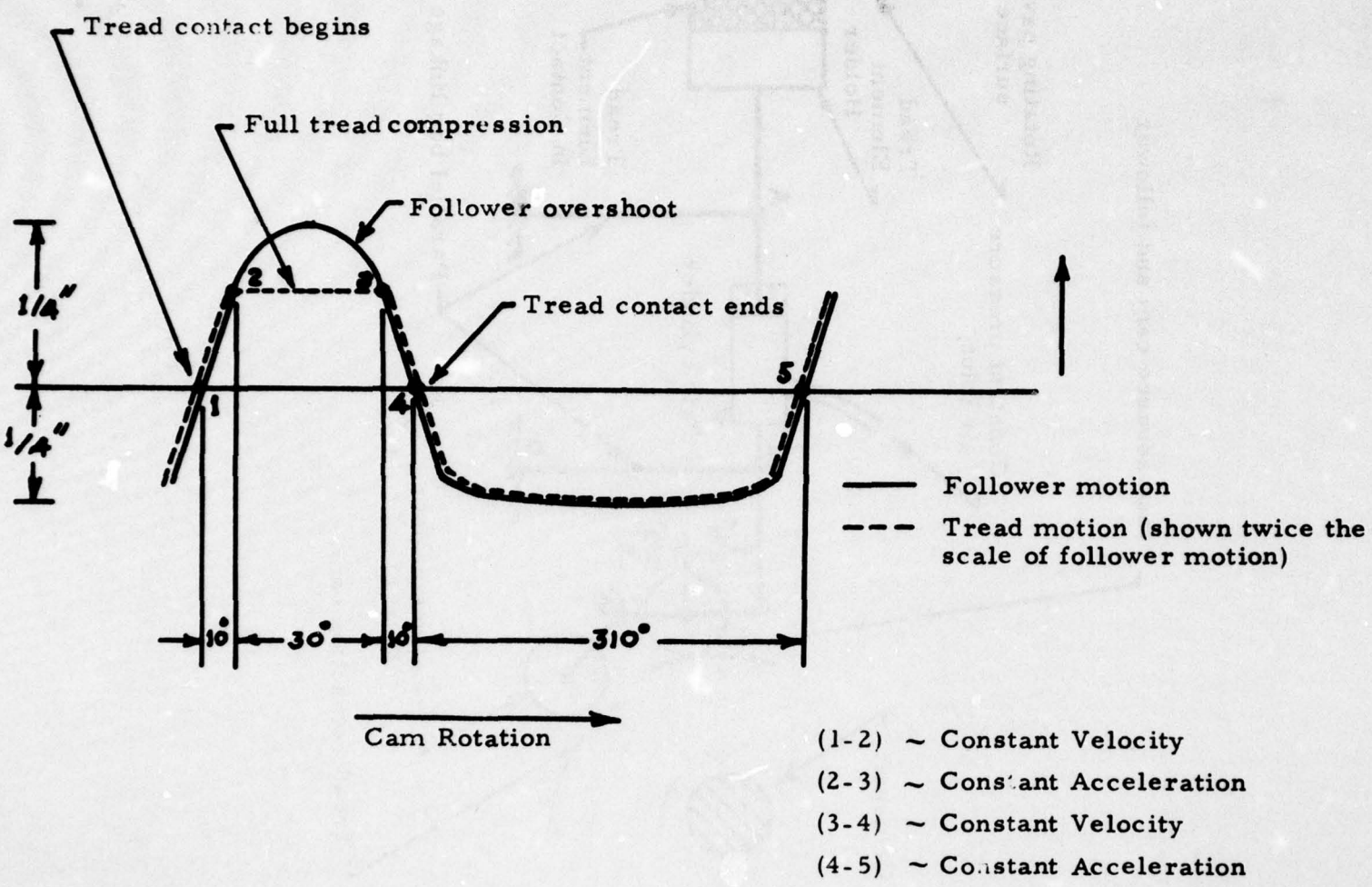

Figure 19 Follower Motion

is being compressed against the pavement, the tread force will build up gradually. During the motion (2-3), the tread is fully loaded against the pavement and the follower is decelerating, so the loading will consist of the tread load and the inertia load. During (4-5), only inertia loads will be present, but since the duration of this motion is 10 times greater than motion (1-3), the inertia force will be much smaller. Thus, the most severe cam loading occurs during motion (2-3).

The largest inertia loads will occur when testing the smaller tires at high speeds. For a 20x4.4 tire, the contact time at a speed of 150 mph is 0.003 sec. (Table III). The force on the tread element will be 432 lbs., and it will compress the tread about 0.075 in. The reaction at the follower will be twice as large because its moment arm is half as long. From Figures 18 and 19, the follower velocity in region (1-2) will be

$$V_f = \frac{3\delta}{2t} \tag{23}$$

where δ is the deflection of the element

and t is the contact time.

Evaluating this equation, the velocity during motion (1-2) will be 3.1 ft/sec.

While the tread is in contact with the pavement, the follower decelerates. The constant deceleration during this part of the motion (2-3) is

$$a_f = \frac{2V_f}{t} \tag{24}$$

where a_f is the follower deceleration

V_f is the follower velocity

and t is the contact time.

Evaluating this expression, the follower deceleration is 65 g's.

The weights of the various components have been estimated, and are given below.

Tread Element Holder	W_T	= 1.8 lbs.
Link AB	W_{AB}	= 1 lb.
Link CD	W_{CD}	= 1 lb.
Followers	W_F	= 15 lbs.
Other moving parts	W'	= 3 lbs.

Because links AB and BC are oscillating, the effective mass at the free end is 1/3 of the total mass. The equivalent weight at the follower pivot is thus,

$$W_{eq} = W_F + 2\,(W_{CD}/3 + W') \tag{25}$$

The weight of the tread holder and the link AB have not been included in the above expression, because they do not form a part of the accelerating system during the period of high loading. From Equation (25), the equivalent follower weight is 21.6 lbs. and the inertia force on the follower is $W_{eq} \times a_f = 1400$ lbs. The net follower force consists of the friction force minus the inertia force. This force is 1400-864 = 536 lbs.

For a larger slower tire, the tread force will be larger than the inertia force. For instance, the contact force of the 56x16 tread element will be about 3,500 lbs. The reaction at the follower will be 7000 lbs., which is near the upper limit for the machine. The inertia force will tend to reduce this follower reaction, so that a conservative design calculation can be made without subtracting this quantity. Thus, the peak force between the cam and follower will be less than 7000 lbs.

The cam loading and speed has been used to determine the specifications of the cams and followers. A nominal cam diameter of 8 inches and a follower diameter of 3 inches have been chosen. A face width of 2 in. will be adequate, as shown below. The maximum compressive stress[6] between two cylindrical bodies in contact (17) is

$$\sigma_c \simeq .591 \sqrt{pE\left(\frac{D_1 + D_2}{D_1 D_2}\right)} \tag{26}$$

where p - force per unit face width

E - Youngs Modulus

D_1 - cam diameter

and D_2 - follower diameter

Evaluating the above equation, the maximum stress is 130,000 lb/in^2. This value is an upper bound obtained for the 56x16 tire after neglecting the reduction due to inertia forces. For all other tires (see Table V), the tread element force is less than one-half that of the 56x16 tire. For all these cases, the maximum follower stress will be under $130,000/\sqrt{2} = 92,000$ lb/in^2, which is well within the endurance limit of the material.

---

[6] For a Poisson's ratio of 0.3.

b. The Drive System

Unlike the pavement drive system, the average torque requirements for the tread element drive will be small. The only energy dissipation in this system will be bearing friction, tread hysteresis and windage loss. Motor power will be needed to decelerate the camshaft to simulate the slow down of the tire during landing. The periodic advance and retraction of the tread will cause significant variations in the instantaneous torque. Therefore, a flywheel will be required to reduce the fluctuations in speed.

A sketch of the tread element drive system is shown in Figure 20. The cams are supported between two bearings, and an overhung flywheel is mounted on one end of the shaft, together with a pulley which transmits the power from the motor through a belt drive. A 15 hp 2500 rpm variable speed regenerative dc motor has been chosen to power the tread element drive. The speed of the cam shaft is reduced to 1250 rpm through a 2:1 reduction in the belt drive. This will be adequate for most tires. However, by changing the pulleys, a different camshaft speed can be obtained. This may be required, for instance, to test small, high-speed tires.

The required motor capacity can be determined with the help of an estimate of the torque fluctuations that occur and the deceleration needed when testing large tires. The peak torque variation will occur during the initial part of the test. For the 56x16 tire, at a landing speed of 150 mph, the contact time is .01 sec. and contact frequency is 15 hz (Table III). The tread element force is 3580 lbs. (Table V). For this tire, the inertia forces on the tread loading mechanism will be small compared to the normal load. Since these inertia forces oppose the load, a conservative design estimate can be obtained by neglecting their effects. Under these loading conditions, the cam profile and linkage geometry have been analyzed to determine the torque fluctuations of the camshaft. This is shown in Figure 21. Although the actual torque curves are not pure sine waves, the <u>area</u> under the curves will be very close to the value obtained with a sinusoidal approximation.

The time constants for the motor will be larger than the period of the fluctuations. Therefore, there will be no appreciable change in motor torque during the torque variation cycle. Under these conditions, the torque equation is

$$I \frac{d\omega}{dt} = T \qquad (27)$$

where I - flywheel inertia

ω - camshaft speed

T - (instantaneous) torque

and t - time.

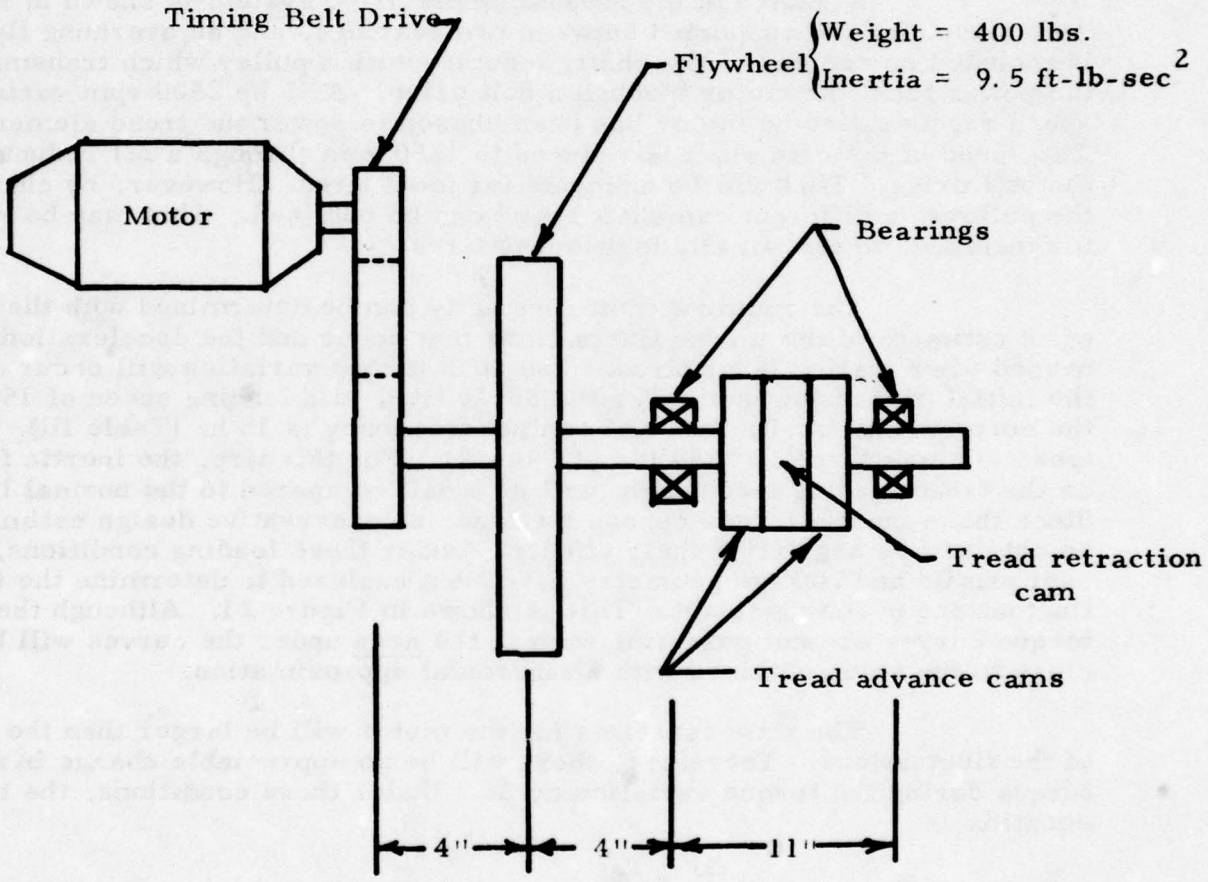

Figure 20 Layout of Tread Element Drive System

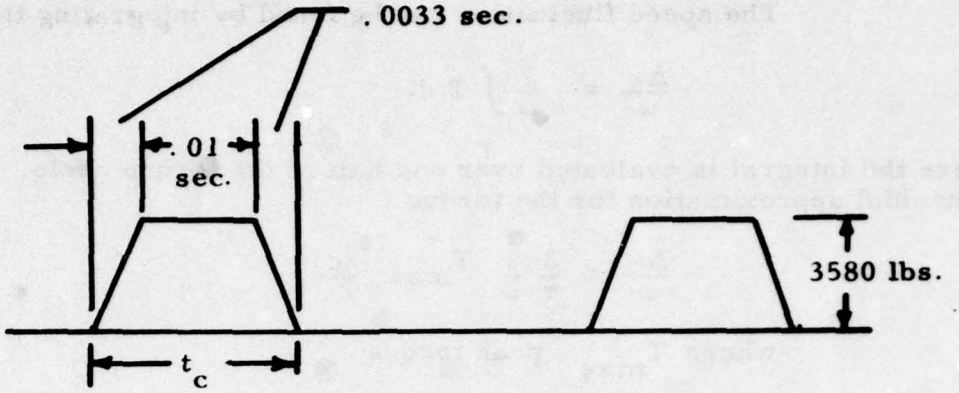

(a) Tread Force at Pavement

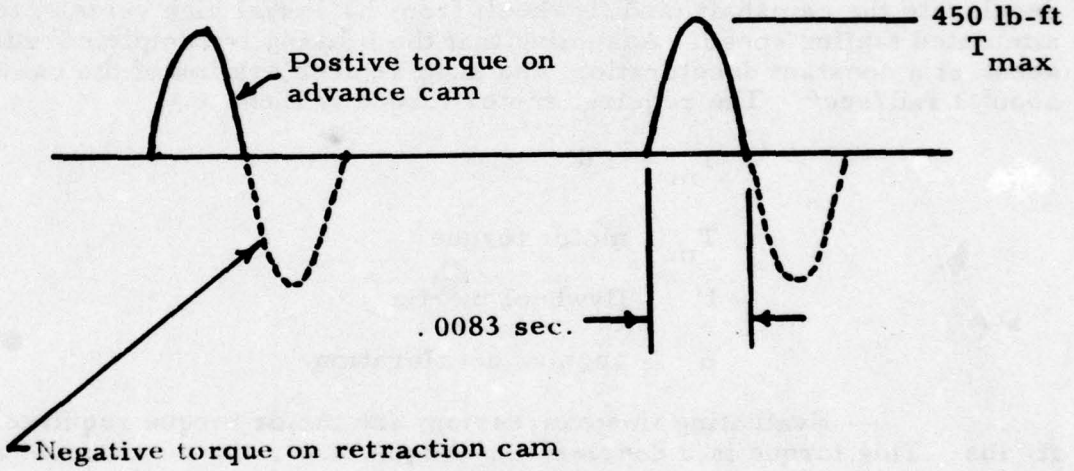

(b) Tread Torque on Camshaft

Figure 21 Camshaft Torque Fluctuations

The speed fluctuation can be found by integrating this equation.

$$\frac{\Delta\omega}{\omega} = \frac{I}{\omega} \int T \, dt \tag{28}$$

where the integral is evaluated over one half of the torque cycle. With a sinusoidal approximation for the torque

$$\frac{\Delta\omega}{\omega} = \frac{2}{\pi} \frac{I}{\omega} T_{max} \frac{tc}{2} \tag{29}$$

where T_{max} - peak torque

and t_c - contact time

For the flywheel chosen (I = 9.5 ft-lb-sec^2), the above expression shows that the speed variation of the camshaft during the high speed part of the landing simulation will be less than 1%.

Over the course of the test, the motor torque is required to decelerate the camshaft (and flywheel) from its initial high velocity to the simulated taxiing speed. Assuming that the braking is completed within 30 secs. at a constant deceleration, the angular deceleration of the camshaft is about 3 rad/sec^2. The required motor torque is then

$$T_m = I \alpha \tag{30}$$

T_m - motor torque

I - flywheel inertia

α - angular acceleration.

Evaluating this expression, the motor torque required is 28.5 ft. lbs. This torque is a decelerating torque, i.e., the motor must act as a brake. This is the main reason for choosing a regenerative motor, where braking as well as accelerating torques can be accurately controlled. The peak motor power, occuring at the start of the test (N = 900 rpm), is

$$P = \frac{2\pi NT}{33000} = \frac{2\pi \times 900 \times 28.5}{33000} = 5 \text{ hp.}$$

As with the pavement drive, a motor of higher capacity has been chosen -- in this case, 15 hp. The other motor characteristics are similar to those of the pavement drive motor.

5. INSTRUMENTATION

The instrumentation system measures the forces and moments acting on the tread element, the contact frequency, slip velocity, displacement and bulk temperature of the tread, and the pressure in the air cylinder. From these measurements, the friction coefficient can be found. The mean wear (over the whole element) can be calculated from the readings of tread displacement, while the total wear can be found by weighing the tread element before and after the test(s). Comparison of the mean and the total wear will indicate the extent of any nonuniformities that may be present (e.g., misalignment) and will serve as a guide for further adjustment or modification.

In addition to the basic friction and wear measurements, the forces and moments acting on the tread element will also be measured dynamically. This capability allows the machine to be used to study selected friction and wear effects in greater detail.

The following measurements will be made.

(1) Friction force

(2) Normal force

(3) Lateral force

(4) Pitching moment

(5) Rolling moment

(6) Yawing moment

(7) Tread displacement (compression)

(8) Bulk temperature

(9) Cylinder pressure

(10) Pavement speed

and (11) Contact frequency.

The instrumentation system consists of the sensors, the signal conditioning circuitry and the recording equipment. All the data obtained during the test will be recorded for subsequent analysis and evaluation. The sensors, conditioning circuitry and recording equipment are described in the following paragraphs.

a. Sensors

The force and moment measurements, (1) through (6) in the previous section, will be made with strain gages mounted on the tread holder and loading linkage. Tread displacement, which gives the compression under the inflation pressure force, will be measured with a Linear Variable Differential Transformer (LVDT). The bulk temperature of the element will be monitored with a thermocouple embedded within the carcass. Cylinder pressure will be measured with a pressure transducer, and the pavement velocity and contact frequency will be obtained directly from the tachometer feedback signals of the two drive motors. The locations of the strain gages, thermocouple and LVDT are shown in Figure 22. The individual gages used to measure the various forces and moments are also identified.

b. Signal Conditioning Circuitry

The signals from the sensors have to be amplified and processed to be compatible with the visual readout and recording equipment. This function is carried out by the conditioning circuitry shown in Figure 23. Amplification is obtained with standard instrumentation amplifiers. The usual null and gain controls are provided to facilitate calibration and readout. The output of the instrumentation system is monitored with the help of a meter display. This visual readout will be used primarily during calibration and adjustment prior to the test. During the test the signals will be recorded on an 11 channel optical chart recorder, which will provide a permanent record for subsequent evaluation. Alternatively, the data can also be recorded and stored on magnetic tape.

The speed of the pavement and the tread loading duration and frequency will be controlled during the test by a Data-Track programmer. When curves of slip velocity and aircraft speed are programmed into the machine, the pavement and cam speeds will be established. The control can then be transferred to the programmer and the test will proceed automatically.

6. OTHER SYSTEMS

A sprinkler system has been provided to wet the pavement surface. It is expected that the water output will be sufficient to cover the smaller surface irregularities (about 1/64 in. or less) and thereby help investigate the effects of wet runway landings on tire friction and wear. A series of nozzles in front of the tread element will spray the rotating pavement with water. The exact size and location of the nozzles will be determined during the initial experiments with the machine.

As discussed in Section I, pavement contamination with this new design is expected to be significantly less than that occurring with conventional drum dynamometers. A decontamination system has been provided to further reduce the contamination level. Prior to the test, the pavement should be cleaned with a commercial runway cleaning solution. During the test, a rotating wire or bristle brush will be used to reduce the surface contamination.

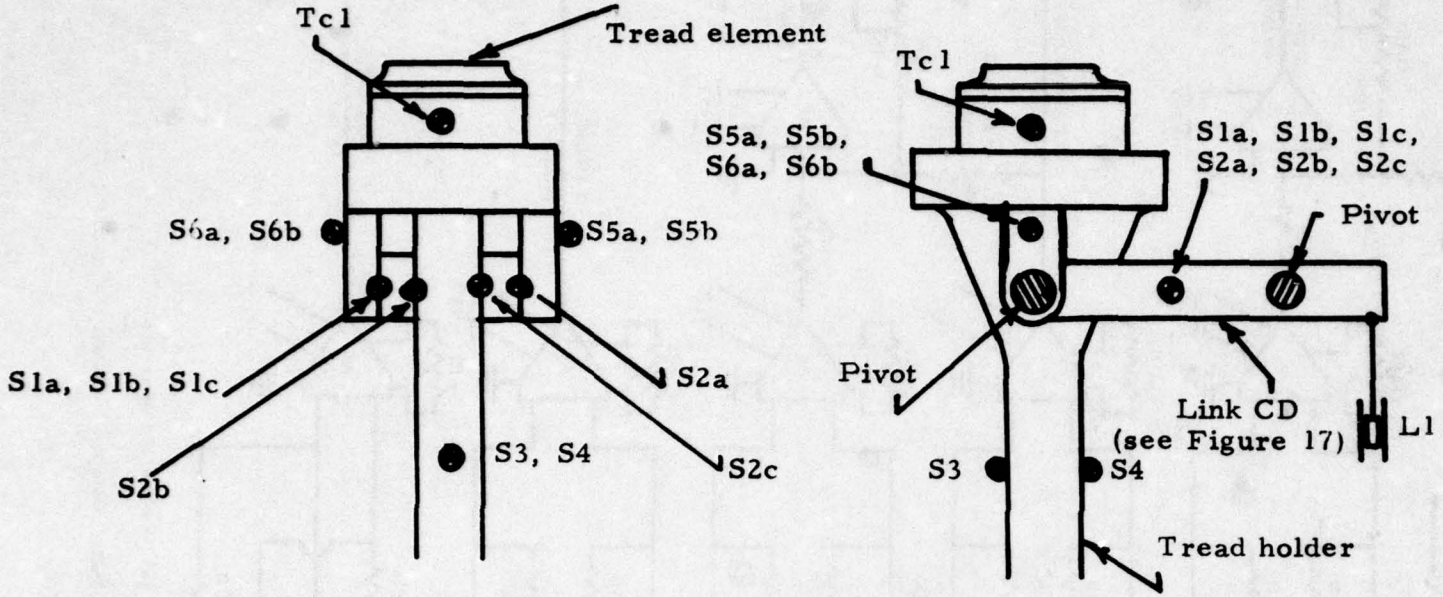

1a, 2a	- Friction Force
5a, 6a	- Normal Force
1b, 2b	- Transverse Force
1a, 2a, 3, 4	- Pitching Moment
1b, 2b, 5b, 6b	- Rolling Moment
1c, 2c	- Yawing Moment
L1	- Tread Displacement
Tc1	- Tread Bulk Temperature

Figure 22 Location of Sensors

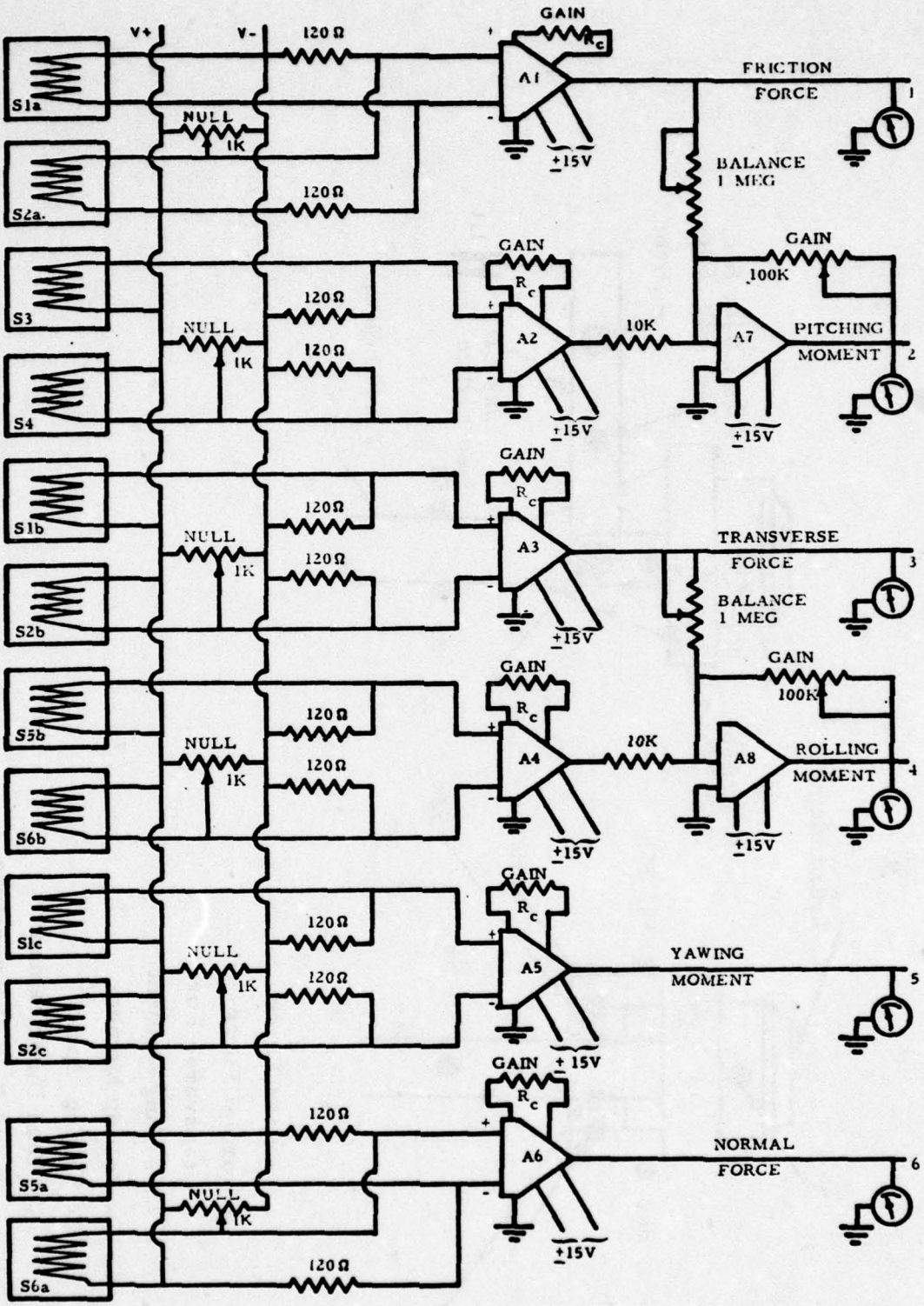

(a) Forces and Moments

Figure 23 Instrumentation System

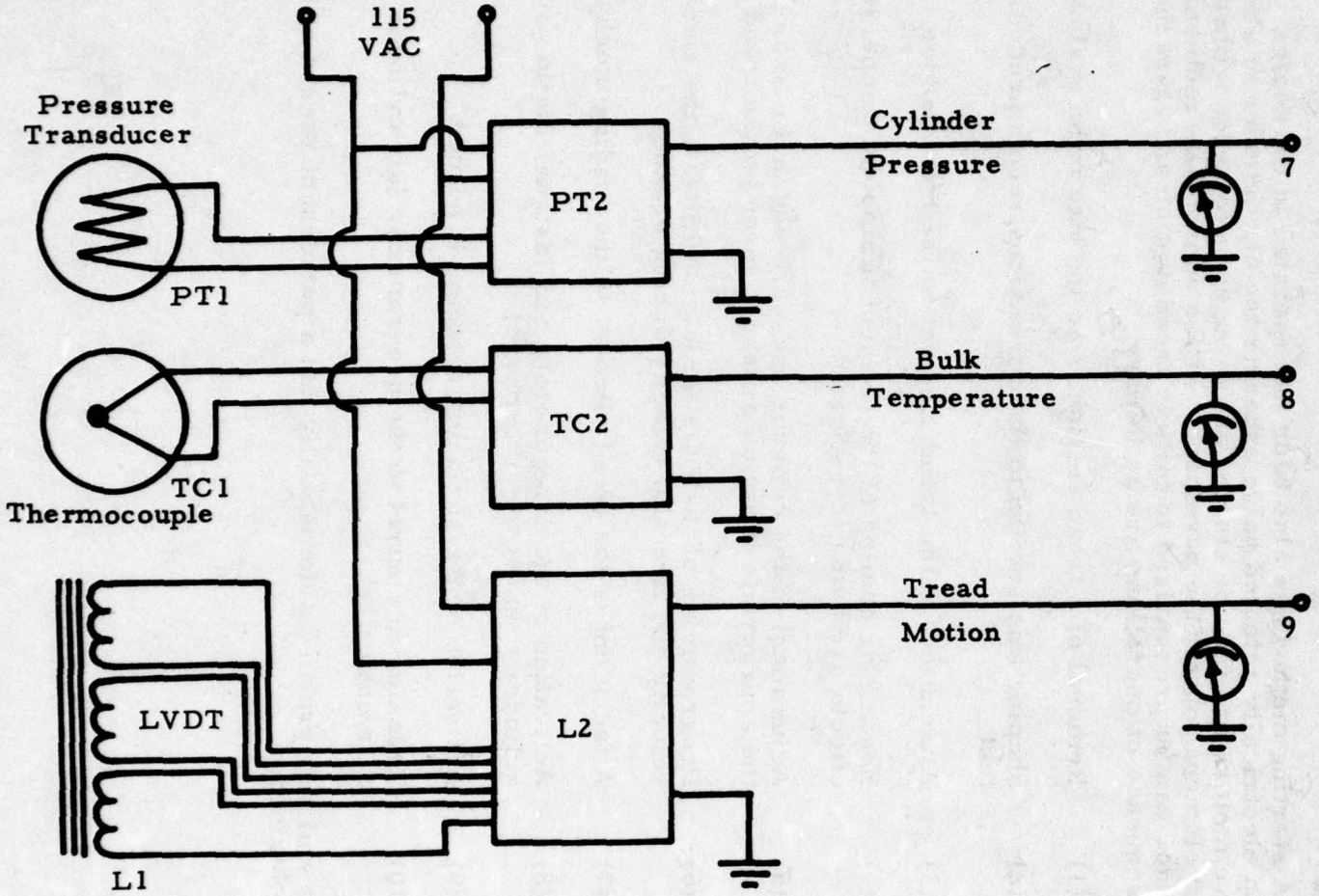

(b) Pressure, Temperature and Motion

Figure 23 --- Concluded

The preceding sections have described the subsystems of the machine. An overall view of the assembly is shown in Figures 24 and 25.

A starting method has also been incorporated in the design. At the start, an electrically actuated valve exhausts the air cylinder to atmosphere. The drive motors can then be started and brought up to speed without having the tread element contact the pavement. At the appropriate moment, the air cylinder can be pressurized to initiate tread motion and start the test. A typical sequence of operations are as follows.

(1) Removal of a tread section from the tire to be evaluated.

(2) Shaping this section to the dimensions recommended for the test.

(3) Attachment of the tread element to the tread holder.

(4) Heating or cooling of the element if ambient temperature effects are being investigated.

(5) Adjustment of the cylinder pressure regulator to simulate the appropriate inflation pressure force on the tread element.

(6) Programming of the Data-Track to simulate the aircraft velocity and tire slip velocity during braking.

(7) Attachment of the tread element to the loading mechanism.

(8) Activation of the drive motors and instrumentation system (air cylinder exhaust to atmosphere).

(9) Activation of the sprinkler system, if needed.

(10) Transfer of control to the programmer (air cylinder pressurized automatically).

The test will now proceed automatically and a permanent record of the data will be obtained.

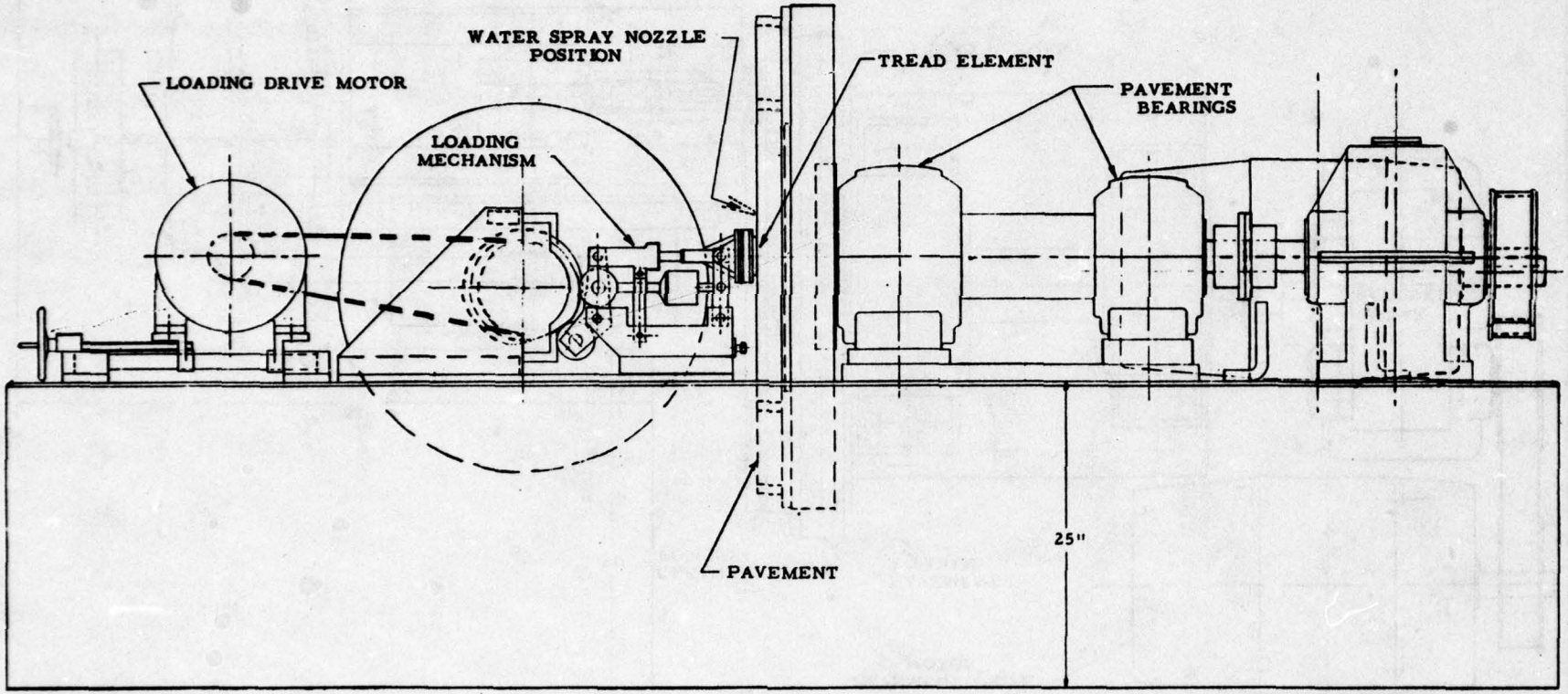

Figure 24 Side View of Tire Tread Testing System

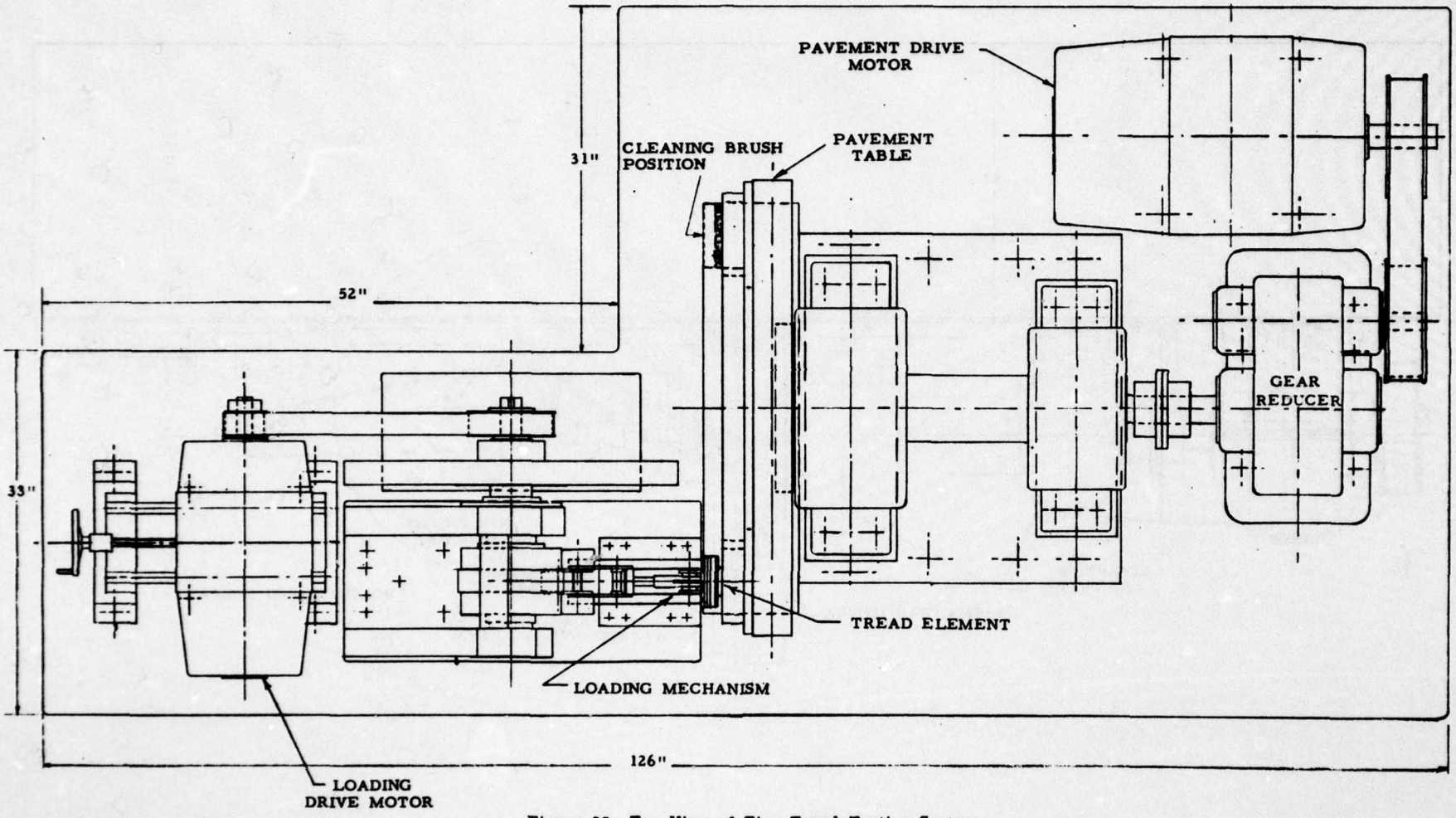

Figure 25 Top View of Tire Tread Testing System

SECTION VI

CONCLUSIONS AND RECOMMENDATIONS

The results of this study indicate that it is feasible to evaluate the primary friction and wear characteristics of an aircraft tire by testing a small element of the tread. An analysis of tire service has confirmed that most of the normal tread wear occurs during the landing deceleration. For this condition the significant variables that affect tire friction and wear have been identified. A test method has been developed to simulate the effects of these parameters for a tread element obtained from the tire. This approach reduces the size and cost of the test equipment but, unlike most reduced scale methods, does not require any test samples of special manufacture.

A prototype machine has been designed to implement this method and record the test data. An artist's impression of this design is shown in Figure 26. The machine will be able to test tires of all sizes over the normal range of touchdown velocities and braking slip. The output data from the tests will consist of the friction force and the wear of the tread element during a simulated landing. The other forces and moments and the motion of the element will also be measured and recorded. Provision has been made to simulate a number of different landing conditions, including wet runways and low temperature operation. The results obtained from these tests can be used to estimate the stopping distance and wear life of the tire under various service conditions. The machine can also be used for experimental studies of selected friction and wear phenomena to contribute to a better understanding of tire performance.

By developing this test method, additional tire specifications can be determined to help evaluate tire braking performance and tread life. Such specifications will reduce the number of flight tests presently needed to compare alternate tire designs.

The tread testing concept developed in this program has several potentially attractive features that could improve present tire testing procedures. The test equipment is likely to be smaller and less expensive than conventional test machinery. Analytical estimates indicate that pavement contamination will also be reduced. The friction and wear data obtained during a simulated landing will lead to a more realistic laboratory evaluation of tire performance. These test data can also be used to compare different tread compounds on the basis of wear life and stopping distance.

Thus, there are strong indications that the tread testing method developed in this program can lead to improved tire evaluation by providing simulated friction and wear data quicker and at a lower cost. Therefore, it is recommended that this effort be carried to the next stage of development which includes fabrication of the prototype testing machine and demonstration of its capabilities.

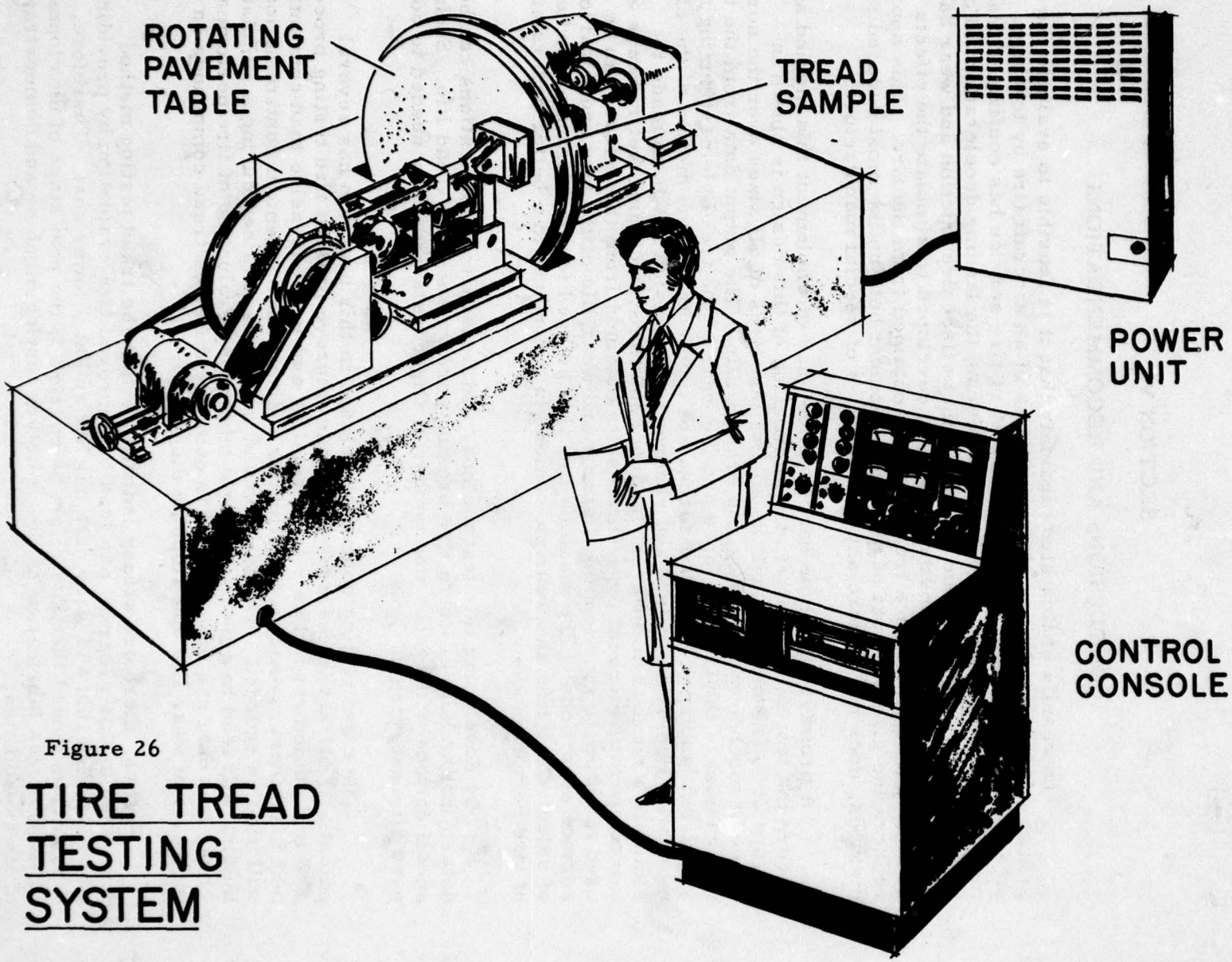

Figure 26

TIRE TREAD
TESTING
SYSTEM

APPENDIX I

CONTAMINATION ANALYSIS

In this appendix, a simple expression is developed to compare the average thickness of the contaminant layer for a conventional rotating drum tire tester and the new tread element testing concept.

1. ROTATING DRUM TIRE TESTER

The volume of tread worn away during a simulated landing is

$$v = \pi \, d \, b \, t \tag{1}$$

where d is the tire diameter, b is the width of the footprint and t is the average tread depth worn away.

The heat and pressure in the contact zone causes some of this abraded rubber to adhere to the drum and contaminate the surface. The average thickness of the contaminant layer (x_1) is

$$x_1 = k_1 v / [\pi D_1 b] \tag{2}$$

where D_1 is the diameter of the drum, and k_1 is the fraction of the abraded rubber that adheres to it.

Substituting for v from Equation (1), the average layer thickness is

$$x_1 = k_1 (d/D_1) \, t \tag{3}$$

2. TREAD ELEMENT TESTING MACHINE

For the new machine, the volume of tread worn away in a simulated landing is

$$v = \ell w t \tag{4}$$

where ℓ is the length of the tread element and w is the width.

The average thickness of the contaminant layer is

$$x_2 = k_2 v / [\pi D_2 w] \tag{5}$$

where k_2 is the fraction of the abraded rubber that adheres to the pavement table, and D_2 is the table diameter.

Substituting for v from Equation (4)

$$x_2 = k_2(\ell/\pi\ D_2)t \tag{6}$$

The relative contamination severity for each machine can be found by comparing the average contaminant thicknesses

$$x_1/x_2 = (k_1/k_2)\ (\pi d/\ell)\ (D_2/D_1) \tag{7}$$

The ratios k_1 and k_2 will depend on the roughness of the surfaces, the heat generated within the contact zone, the normal pressure, etc. Although these ratios cannot be determined analytically, it is likely that they will be of the same order. Therefore, as a first approximation, the ratio k_1/k_2 can be set equal to unity.

The contamination ratio is now

$$x_1/x_2 = (\pi d/\ell)\ (D_2/D_1) \tag{8}$$

Usually, the tire diameter is between 2 ~ 4 ft while the element length will be about 2 ~ 4 inches, so that the ratio $\pi d/\ell$ is about 36. The table-to-drum diameter ratio D_2/D_1 depends on the relative sizes of the two machines. Typically, this ratio will lie between 0.1 ~ 0.5, so that the contamination ratio x_1/x_2 will be between 4 ~ 20.

This analysis is approximate. The results, however, do indicate that the tread element testing concept is significantly less prone to pavement contamination than the rotating drum tire tester.

APPENDIX II

TIRE FRICTION LOSS ESTIMATES

This appendix describes the analyses used to estimate the relative magnitudes of braking, spin up, cornering and takeoff friction loss. The purpose of these analyses is to identify which of the above loading conditions contribute significantly to tread wear. In this way, we can concentrate on studying and simulating the significant causes of wear, rather than every loading condition of the tire.

In most instances, tread wear is estimated through semi-empirical analyses together with experimental correlation. For the present purpose of identifying the dominant loading conditions, an analytical approach is convenient.

Tread wear is caused by frictional energy dissipation in the contact zone, due to relative motion at the tread-runway interface. The frictional energy loss is thus a measure of the wear, and can be used to distinguish between the high and low wear loading conditions of the tire. This is carried out below.

1. BRAKING

A sketch of the tire under braking torque is shown in Figure 27. If the tire is rolling without slip, like a toothed wheel on a track (Figure 27b), this force does no work. Hence, there is no frictional energy loss.

During braking, there is always some slip at the tread-runway interface. The relative motion results in work being done by the friction force. The frictional energy loss E_B, which is equal to the work done by the friction force F_B, is

$$E_B = \int F_B \, dx \tag{1}$$

where x is the slipping distance, and the integral is evaluated over the length of the braking roll. For a given slip s,

$$dx = Vs \, dt \tag{2}$$

where V is the aircraft velocity and t is the time. Introducing the friction coefficient μ, the friction force is

$$F_B = \mu W \tag{3}$$

where W is the weight supported by the tire. Substituting Equations (2) and (3) into Equation (1), the friction loss is

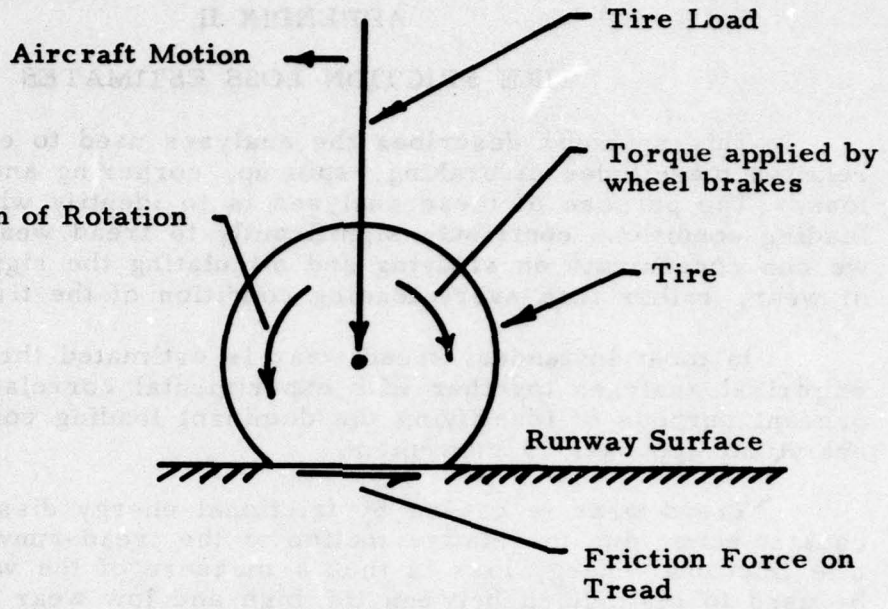

(a) Forces, Torques and Motion of a Braked Tire

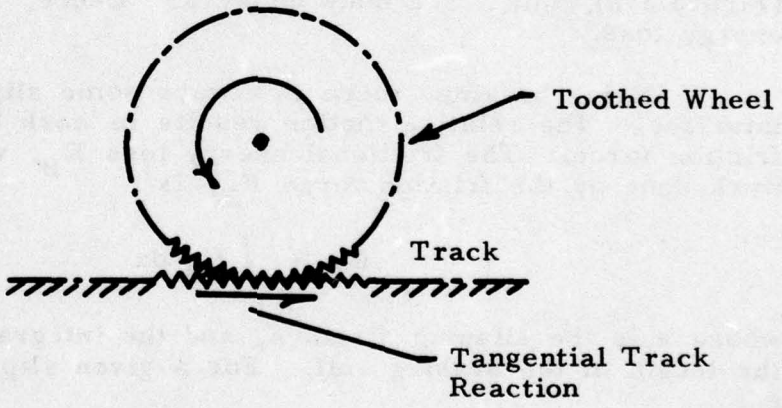

(b) Toothed Wheel Analogy

Figure 27 Load Diagram of Braked Aircraft Tire

$$E_B = \int \mu \; W \; Vs \; dt \tag{4}$$

During most of the landing roll, μ, W, and s are fairly constant. Therefore

$$E_B = \mu \; W \; s \int V \; dt \tag{5}$$

The integral in Equation (5) is easily seen to be equal to the landing distance L. Thus

$$E_B = \mu \; W \; s \; L \tag{6}$$

With the assumptions of constant decelerating force (i.e., constant μ and W), the landing distance is

$$L = \frac{V^2}{2g\mu} \tag{7}$$

From Equations (6) and (7)

$$E_B = \left(\frac{WV^2}{2g}\right) s \tag{8}$$

The term in parentheses is the initial kinetic energy of the aircraft $(KE)_a$.

Thus, the frictional energy loss during landing is

$$E_B = (KE)_a \; s \tag{9}$$

Since the slip (s) during braking is usually between 0.15 ~ 0.2, the energy dissipated by the tires due to braking (during landing) is 15 percent ~ 20 percent of the initial kinetic energy of the aircraft. The remaining energy is dissipated in the brake shoes and drums.

This above analysis can also be used to estimate the tire friction loss during takeoff. In this situation, the tires are practically rolling free. However, deformation of the (curved) tread as it enters the (flat) footprint results in some relative motion at the interface. This motion, roughly speaking, corresponds to an equivalent slip s of about 0.005 (3). An estimate based on Equation (9) shows that about 1/2 percent of the lift-off kinetic energy is lost through tire friction during takeoff.

2. SPIN UP

Spin up is that part of the landing sequence during which an initially non-rotating tire is brought up to speed by contact with the

runway. In a fraction of a second, the rotational speed of the tire increases from zero to that corresponding to the landing speed of the aircraft. The slip changes from a high value (s = 1) at the beginning of touchdown to essentially zero when the wheel has reached full speed. The presence of high relative velocities suggests that high wear rates may be present. However, the short duration of spin up indicates that the actual wear may be small.

During spin up, assuming that the wheel brakes are not applied, the torque T on the tire is related to the angular acceleration $\ddot{\theta}$ of the wheel as follows.

$$T = \frac{I}{g} \ddot{\theta} \tag{10}$$

where I is the moment of inertia of the wheel and g is the acceleration due to gravity.

During spin up, the torque on the wheel varies with time. It can be expressed as

$$T = \mu W' r \tag{11}$$

where μ is the friction coefficient, r is the effective tire radius and W' is the (time dependent) load on the tire.

In practice, μ, r and W' will vary during spin up. The variation in μ and r will not be large, and as a first approximation, they can be considered constant. The tire load will vary from zero at the start of touchdown to the equilibrium tire load (approximately) at the completion of spin up.

In order to proceed further with the analysis, it is necessary to know the variation of tire load with time. A reasonable approximation is to assume that the sink rate during spin up is constant. Since the wheels are attached to the airframe through a flexible (spring-dashpot) strut, the tire load during spin up will increase fairly linearly with time. This relationship can be written as

$$W'/W = t/t' \tag{12}$$

where W is the equilibrium wheel load, t' is the spin up duration and t is the time.

Equations (10) to (12) can be solved to give the number of wheel rotations θ' for completion of spin up.

$$\theta' = (1/3 \mu \pi) (w/W) (k/r)^2 (V^2/gr) \tag{13}$$

In the above equation, the first term depends only on the friction coefficient and has a value between 0.2 ~ 0.5. The second term is the ratio of the wheel weight to the wheel load, which is typically about 1/100. The third term is the ratio of the radius of gyration to the (geometric) radius of the wheel. Approximating the wheel as a solid disk this ratio is about 0.7. The fourth term, which depends on the touchdown velocity and the tire radius, has a value between 500 ~ 1000. Substituting these typical values into Equation (13), it is found that spin up is completed within about one wheel revolution, so that spin up wear should be fairly evenly distributed around the tire periphery.

The distance L' travelled by the aircraft during spin up is also of interest. From Equations (10) to (12) this distance is

$$L' = (2/\mu)\ (w/W)\ (k/r)^2\ (V^2/g) \tag{14}$$

With a typical value for μ of 0.5 and a touchdown speed of 120 mph, the spin up distance is

$$L' \simeq 22 \text{ ft} \tag{15}$$

The high wear rate during spin up is likely to cause significant rubber deposit and discoloration in the touchdown areas of the runway. Observations of the landing scrub marks at Wright Patterson AFB show that these are about 30 ft long. This observation compares favorably with the estimated spin up distance of 22 ft and confirms the validity of the earlier assumptions.

The frictional loss E_s can now be calculated as follows.

$$E_s = \int T\, d\phi \tag{16}$$

where ϕ is the wheel rotation due to tire slip, and the integral is evaluated over the spin up distance. This can also be written as

$$E_s = \int_0^{t'} \frac{T}{r}\ (V - r\,\dot{\theta}\,)\ dt$$

where the upper limit t' is the time for completion of spin up.

Substituting for T from Equation (10) and simplifying, the energy loss is

$$E_s = \int_0^{V/r} \left(\frac{I}{gr}\right)\ (V - r\dot{\theta})\ d\dot{\theta} \tag{17}$$

During spin up, the aircraft speed V will be essentially constant, since the kinetic energy needed to accelerate the wheels is very small compared to the kinetic energy of the aircraft. With this assumption, Equation (17) can be integrated to give the frictional loss due to tire spin up.

$$E_s = (I/2g)\ (V/r)^2 \tag{18}$$

This expression shows that the energy loss due to tire spin up is equal to the kinetic energy needed to bring the wheel up to speed. The spin up process is thus 50 percent efficient. Half the energy is spent in accelerating the wheel while the other half is lost in tire friction.

It is instructive to compare the spin up energy loss with the braking energy loss. From Equations (8) and (18)

$$E_s/E_B = (k/r)^2\ (w/W)/s \tag{19}$$

After substituting typical values for the parameters in the above equation, the energy loss ratio is

$$E_s/E_B \simeq 0.02 \tag{20}$$

The above result indicates that tire friction losses during spin up are only about 2 percent of the losses during braking. From this, we can also conclude that spin up wear is negligible compared to the wear during braking.

3. CORNERING

Cornering and parking maneuvers can result in tread wear. There are two reasons why cornering wear is difficult to estimate.

(1) Cornering is a more complex loading condition than straight braking. There are several additional factors that enter into the analysis, such as yaw angle, lateral slip, etc. The analysis is therefore more difficult.

(2) Cornering wear is highly dependent on the layout of the runways and taxiways, the type of aircraft and the ground handling technique. This does not allow cornering wear to be treated with the same generality as braking wear.

To obtain an indication of the relative magnitude of cornering wear, the effects of a single 90° turn have been evaluated. A sketch of the aircraft landing and turning sequence is shown in Figure 28. It is assumed that the turn is made at one-tenth of the touchdown velocity with a constant radius of one-tenth the landing run.

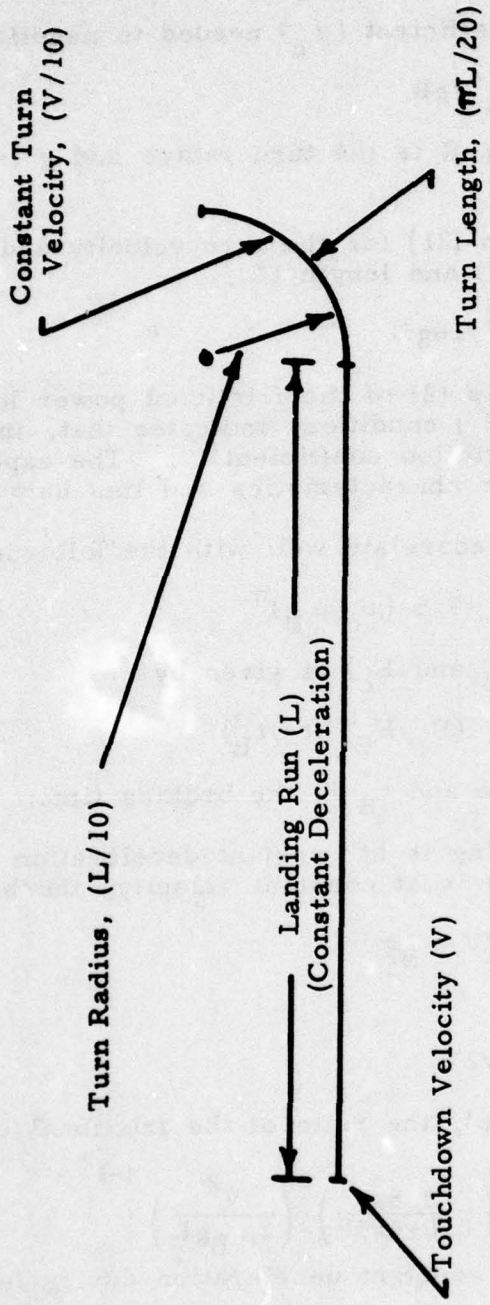

Figure 28 Assumed Landing and Turning Sequence

The lateral friction coefficient (μ_c) needed to negotiate the turn is

$$\mu_c = V_t^2/gR \tag{21}$$

where V_t is the turn velocity, R is the turn radius and g is the acceleration due to gravity.

Substituting in Equation (21) for the turn velocity and radius in terms of the landing speed (V) and length (L),

$$\mu_c = V^2/10gL \tag{22}$$

An approximate analysis (2) of the frictional power loss under braking (P_B) and cornering (P_c) conditions indicates that, in both cases, the average loss varies as (friction coefficient)^n. The exponent (n) depends on the runway surface characteristics and lies between 2 and 3.

The experimental data correlate well with the following relationship

$$P_c/P_B = 3.5\ (\mu_c/\mu_B)^n \tag{23}$$

The frictional energy loss (E_B and E_c) is given by

$$E_c/E_B = (P_c/P_B)\ (t_c/t_B) \tag{24}$$

where t_c is the cornering time and t_B is the braking time.

Assuming that the landing is at constant deceleration (with braking coefficient μ_B) and the turning is at constant velocity, the braking time is

$$t_B = 0.9V/\mu_B g \tag{25}$$

and the cornering time is

$$t_c = \pi L/2V \tag{26}$$

From Equation (22) through (26), the ratio of the frictional energy loss in the tires is

$$E_c/E_B = \left(\frac{3.5\pi}{0.9x4x5^n}\right)\left(\frac{V^2}{2\mu_B gL}\right)^{n-1} \tag{27}$$

With the assumption of constant deceleration during landing, the braking distance is

$$L = 0.9V^2/2\mu_B g \tag{28}$$

From Equations (27) and (28), the frictional energy loss can be expressed by a very simple relationship

$$E_c/E_B \simeq \pi/5^n \tag{29}$$

For an average runway, with the value of n midway between 2 and 3,

$$\frac{E_c}{E_B} \simeq 0.056 \tag{30}$$

This indicates that the tire friction loss during a low speed 90° turn will be about 6% of the tire loss during landing. This analysis is approximate, but the conclusion is clear, and shows that normal cornering wear is much less than braking wear.

APPENDIX III

TIRE CONTACT PARAMETER CALCULATIONS

This appendix describes the method by which the tread parameters shown in Table III have been obtained. As an illustration, sample calculations for the 56 x 16 tire are presented. Similar calculations have been carried out for the other tires.

The tire specifications have been obtained from Reference 8. These specifications include

1. The tire outside diameter, D
2. The rim flange diameter, D_f
3. The loaded radius, R_L

and 4. The section width, W

For the 56 x 16 tire, these dimensions are

$D = 56.4$ in. (max.)

$D_f = 32.5$ in.

$R_L = 24.1$ in.

and $W = 16.2$ in. (max.)

The (percentage) radial deflection δ can be obtained from the unloaded and loaded dimensions as follows

$$\delta = \frac{D - 2R_L}{D - D_f} \tag{1}$$

The unloaded section height H is given by

$$H = (D - D_f)/2 \tag{2}$$

For the 56 x 16 tire, the above two parameters are

$$\delta = \frac{56.4 - 2 \times 24.1}{56.4 - 32.5} = 34.3\%$$

and $H = (56.4 - 32.5)/2 = 12$ in.

AD-A069 211 FOSTER-MILLER ASSOCIATES INC WALTHAM MASS F/G 1/3
AN INNOVATIVE FRICTION AND WEAR TEST FOR AIRCRAFT TIRES.(U)
NOV 72 K M CAPTAIN, V K STOKES, J H EDWARDS F33657-71-C-1024
UNCLASSIFIED WP-7141 ASD-TR-72-85 NL

2 OF 2
AD
A069211

END
DATE
FILMED
7-79
DDC

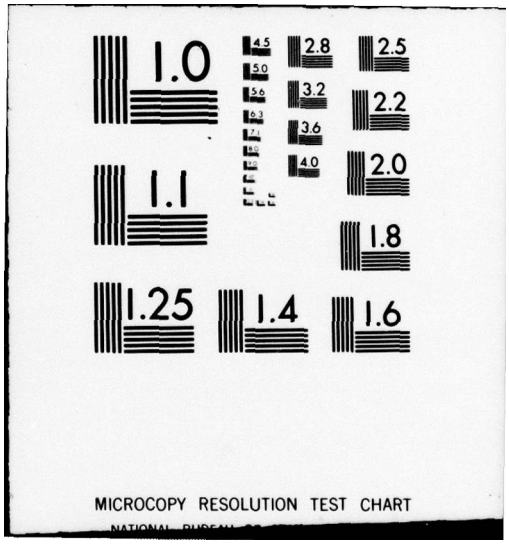
1.0
1.1
1.25
1.4
1.6
1.8
2.0
2.2
2.5
2.8
3.2
3.6
4.0
4.5
5.0
5.6
6.3
MICROCOPY RESOLUTION TEST CHART

The intersection of a horizontal plane through the tire at the radial deflection point results in an eliptical common section ("decap") with the major axis L_d and area A_d given by

$$L_d = 2\sqrt{\delta H(D - \delta H)} \tag{3}$$

$$A_d = 4\delta H \sqrt{(D - \delta H)(W - \delta H)} \tag{4}$$

Due to tire stiffness and bending, the actual footprint length L and area A will be smaller than the decap values (see Figure 29). For modern tires (8), empirical correlations[7] show that the footprint dimensions can be estimated from the decap parameters as follows

$$L = 0.85\, L_d \tag{5}$$

$$A = 0.633\, A_d \tag{6}$$

For the 56 x 16 tire,

$$L = 0.85 \times 2\sqrt{0.343 \times 12\,(56.4 - 0.343 \times 12)} = 25 \text{ in.}$$

$$A = 0.633 \times 4 \times 0.343 \times 12 \sqrt{(56.4 - 0.343 \times 12)(16.2 - 0.343 \times 12)} = 262 \text{ in}^2$$

The contact ratio (tire circumference divided by the footprint length) is $\pi D/L = \pi \times 56.4/25 = 7$.

When the tire is rolling with a velocity V, an element of the tread contacts the ground with a frequency f_c given by

$$f_c = V/\pi D \tag{7}$$

The contact time t_c for this element (i.e., time spent in the footprint) is

$$t_c = L/V \tag{8}$$

---

[7] Alternate correlations for the footprint length and area are also available See Equations (2) and (3) in Section III. These estimates are within 10% of Equations (5) and (6) above.

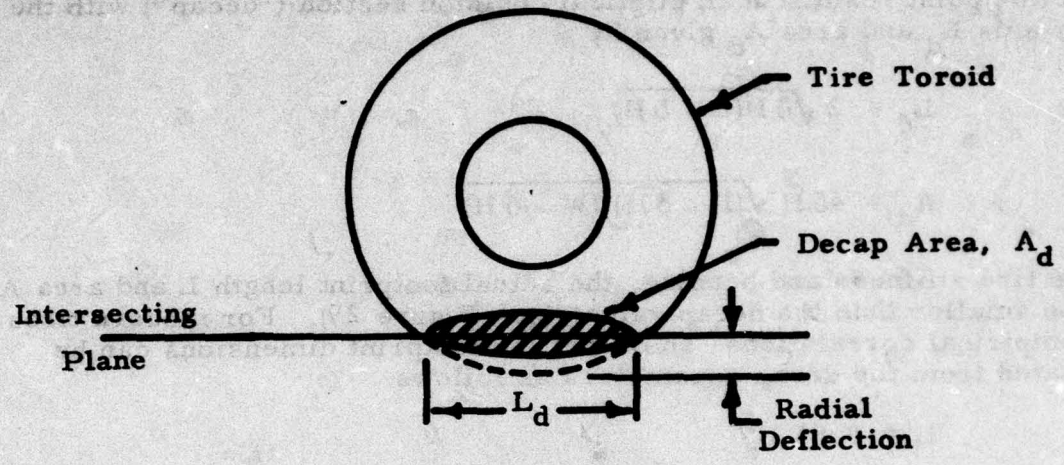

(a) Tire Decap

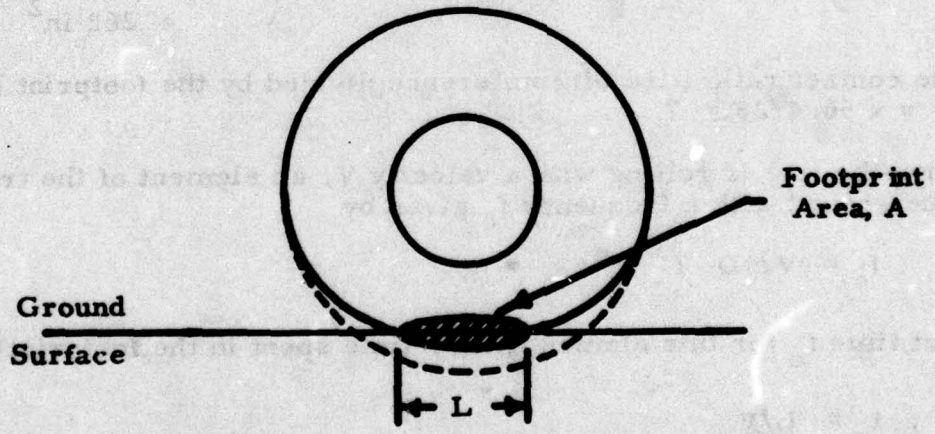

(b) Tire Footprint

Figure 29 Tire Decap and Footprint

For the 56 x 16 tire, with a rolling velocity of 150 mph (220 ft/sec), the contact frequency and contact time are

$$f_c = (220 \times 12)/(\pi \times 56.4) = 15 \text{ hz}$$

and $$t_c = 25/(220 \times 12) = 0.0095 \text{ sec.}$$

For a maximum rated tire speed of 250 mph (366 ft/sec), these parameters are

$$f_c = (366 \times 12)/(\pi \times 56.4) = 25 \text{ hz}$$

$$t_c = 25/(366 \times 12) = 0.0057 \text{ sec.}$$

The above calculations have been carried out for several other tire sizes, and the results are shown in Table III.

REFERENCES

1. Fleeger, D. W., "Tire Wear Index Test," Project No. 156, AD 682360 OONED, Hill AFB, Utah, May 1968.

2. "Friction and Wear in Tires," D. Mat Report No. 157, AD 695807, Edited by W. H. Edwards, Materials Division, Ministry of Technology, UK, June 1969.

3. Mechanics of Pneumatic Tires, Edited by S. K. Clark, Monograph 122, National Bureau of Standards, Washington, D. C., November 1971.

4. Kummer, H. W. and Meyer, W. E., "Rubber and Tire Friction," Engineering Research Bulletin B-80, AD 660927, Department of Mechanical Engineering, The Pennsylvania State University, University Park, Pennsylvania, December 1960.

5. Meyer, W. E. and Schrock, M. O., "Friction of Tires," Presented at ASTM Symposium on Automobile Tire Performance Testing, Atlantic City, New Jersey, February 1968.

6. "Tires, Pneumatic, Aircraft," Military Specification MIL-T-5041E, Department of Defense, Washington, D. C., 14 October 1966.

7. Skele, P., "Rolling Resistance and Carcass Life of Tires operating at High Deflections," Technical Report AFFDL-TR-70-138, Flight Dynamics Laboratory, Wright-Patterson Air Force Base, Ohio, February 1972.

8. Aircraft Tire Engineering Data, B. F. Goodrich Company, Akron, Ohio.

9. Kraft, P., "Force Distribution in the Contact Surface Between Tire and Runway," Technical Memorandum 1365, National Advisory Committee for Aeronautics, Washington, D. C., August 1954.

10. Private Communication, B. F. Goodrich Company, Akron, Ohio, September 1971.

11. Smiley, R. S. and Horne, W. B., "Mechanical Properties of Pneumatic Tires with Special Reference to Modern Aircraft Tires," Technical Note 4110, National Advisory Committee for Aeronautics, Washington, D. C., January 1958.

12. Conant, F. S., "Tire Temperatures," Volume 44, Rubber Chemistry and Technology, American Chemical Society, New York 1971, Pages 397-439.

13. Viehmann, W., "Surface Heating by Friction and Abrasion by Thermal Decomposition," Volume 31, Rubber Chemistry and Technology, American Chemical Society, New York, 1958, Pages 925-940.

14. Rohsenow, W. M. and Choi, H. Y., Heat, Mass and Momentum Transfer, Prentice-Hall, Inc., Englewood Cliffs, New Jersey, May 1963.

15. Private Communication, SKF Industries, Inc., King of Prussia, Pennsylvania, January 1972.

16. Private Communication, Ferguson Machine Company, St. Louis, Missouri, February 1972.

17. Roark, R. J., Formulas for Stress and Strain, McGraw-Hill Book Company, Inc., New York, 1943.

BIBLIOGRAPHY

"Abrasion Resistance of Rubber by the Pico Method," ASTM Specification D 2228-69.

"Aircraft Tires, Technical Standard Order TSO-C62b," Federal Avaiation Agency, Washington, D.C., 29 August 1962.

Campbell, K. L., "Determination of Passenger Car Tire Performance Levels - Treadwear," Paper 690507, presented at the SAE Meeting, Chicago, Illinois, May 1969.

Clark, S. K., "The Rolling Tire Under Load," Paper 650493, presented at the SAE Meeting, Chicago, Illinois, May 1965.

Davis, J. E. and Curry, R. C., "The Cost of Landing an Aeroplane," SAE Paper No. 740C, December 1963.

Domandl, H., "The Braking Characteristics of Airplane Tires," Document No. D6-58384-1TN, AD 683 585, The Boeing Company, Renton, Washington, March 1969.

Fancher, P. S., et al, "Experimental Studies of Tire Shear Force Mechanics," Summary Final Report, PB 201 547, Highway Safety Research Institute, University of Michigan, Ann Arbor, Michigan, July 1970.

Frank, F. and Hofferberth, W., "Mechanics of the Pneumatic Tire," Rubber Chemistry and Technology, Pages 271-322.

Gehman, S. D., "Heat Transfer in Processing and Use of Rubber," Contribution No. 347, Rubber Chemistry and Technology.

Ginn, J. L., Marlowe, R. L. and Miller, R. F., "Tread Wear Operating Variables and Index Determination," Paper 1860, presented at the SAE Meeting, Chicago, Illinois, June 1960.

Grosch, K. A. and Schallamach, A., "Tire Wear at Controlled Slip," Wear, Volume 4, 1961, Pages 356-371.

Luthman, R. R., "Coefficient of Friction of Aircraft Tires on Concrete Runways," WADC Technical Report 55-179, AD 66771, Wright Air Development Center, Wright-Patterson Air Force Base, Ohio, March 1955.

Meades, J. K., "Braking Force Coefficients Obtained with a Sample of Currently Available Radial Ply and Crossed Ply Car Tyres," Report LR 73, PB 176695, Road Research Laboratory, Crowthorne, UK, 1967.

Newton, E. B., Grinter, H. W. and Sears, D. S., "The Pico Laboratory Abrasion Test," Rubber Chemistry and Technology, Volume 34, No. 1, January - March 1961.

Saibel, E. and Tsai, C., "Tire Wear Model - Part 1," Technical Report AFFDL-TR-70-167 Part I, Flight Dynamics Laboratory, Wright-Patterson Air Force Base, Ohio, December 1970.

Savkoor, A. R., "Some Aspects of Friction and Wear of Tires Arising from Deformations, Slip and Stresses at the Ground Contact," Wear, Volume 9, 1966, Pages 66-78.

Sawyer, R. H., Batterson, S. A. and Harrin, E. N., "Tire-to-Surface Friction especially under Wet Conditions," Memorandum 2-23-59L, National Aeronautics and Space Administration, Washington, D. C., March 1959.

Schallamach, A., "Friction and Abrasion of Rubber," Wear, Volume 1, 1957, Pages 384-417.

"Standard Tire for Pavement Tests," ASTM Specification E 249-66.

Schallamach, A., "Recent Advances in Knowledge in Rubber Friction and Tire Wear," Rubber Chemistry and Technology, Pages 209-244.

Schuster, R. and Weichsler, P., "Adhesion between Tire and Roadway," Library Translation No. 1231, AD 819894, Royal Aircraft Establishment, UK, June 1967.

Spinner, S. and Barton, F. W., "Some Problems in Measuring Tread Wear of Tires," Technical Note 486, National Bureau of Standards, Washington, D. C., August 1969.

"Tires," Chemical Week, May 19, 1971, Pages 35-41.

Tomita, H., "Tire-Pavement Friction Coefficients," Technical Report R-672, AD 705987, Naval Civil Engineering Laboratory, Port Hueneme, California, April 1970.

Trivisonno, N. M., "Thermal Analysis of a Rolling Tire," Paper 700474 presented at the SAE Meeting, Detroit, Michigan, May 1970.

Yager, T. J., Sparks, H. C., et al, "A Comparison of Aircraft and Ground Vehicle Stopping Performance on Dry, Wet, Flooded, Slush-, Snow- and Ice-Covered Runways," Technical Note D-6098, National Aeronautics and Space Administration, Washington, D. C., November 1970.

Security Classification

DOCUMENT CONTROL DATA - R & D

(Security classification of title, body of abstract and indexing annotation must be entered when the overall report is classified)

1. ORIGINATING ACTIVITY *(Corporate author)*
Foster-Miller Associates, Inc.
135 Second Avenue
Waltham, Massachusetts 02154

2a. REPORT SECURITY CLASSIFICATION
Unclassified

2b. GROUP

3. REPORT TITLE
AN INNOVATIVE FRICTION AND WEAR TEST FOR AIRCRAFT TIRES.

4. DESCRIPTIVE NOTES (Type of report and inclusive dates)
Final Report, Jun[illegible]71 - Nov[illegible]72,

5. AUTHOR(S) (First name, middle initial, last name)
Khushroo M. Captain, Vijay K. Stokes and John H. Edwards

6. REPORT DATE
Nov[illegible]1972

7a. TOTAL NO. OF PAGES
95

7b. NO. OF REFS
17

8a. CONTRACT OR GRANT NO.
F33657-71-C-1024

8b. ORIGINATOR'S REPORT NUMBER(S)
WP-7141

8c.

9b. OTHER REPORT NO(S) *(Any other numbers that may be assigned this report)*
ASD TR-72-85

8d.

10. DISTRIBUTION STATEMENT
Approved for public release; distribution unlimited.

11. SUPPLEMENTARY NOTES
105p

12. SPONSORING MILITARY ACTIVITY
Deputy for Engineering
Aeronautical Systems Division
Wright-Patterson AFB Ohio 45433

13. ABSTRACT

This program is a first step toward the formulation of a standardized test for aircraft tire friction and wear. A method is determined to evaluate tire performance by testing a small section of the tread. This reduces the size and cost of the test equipment and shortens the test time.

Tread loading during takeoff, landing and cornering has been analyzed in order to identify the operating conditions resulting in the most severe tread wear and friction requirements.

The factors that affect tire friction and wear were studied, and the dominant forces, motions and heating of a tread element during landing were determined. The analysis was then used as a basis for the formulation of the test method and the requirements for the testing equipment.

A machine has been designed to simulate the significant mechanical and thermal loading on the tread element during landing. This machine will be capable of evaluating the full range of current tire sizes under dry and wet runway conditions and ambient temperature extremes. Implementation of this concept should provide a rapid and economical tire testing capability which will evaluate tires on the basis of stopping distance as well as tread life.

142 400

DD FORM 1 NOV 68 1473

Security Classification

14. KEY WORDS	LINK A		LINK B		LINK C	
	ROLE	WT	ROLE	WT	ROLE	WT
Aircraft Tire Traction						
Aircraft Tire Wear						
Tire Testing Method						